Frontiers in Finite Element Procedures & Applications [1]

by

Klaus-Jürgen Bathe
Massachusetts Institute of Technology
Cambridge, MA 02139, USA

Abstract

We consider in this paper some frontiers in finite element procedures, and frontiers of novel applications. We focus on theoretically well-founded procedures that advance the solution of practical problems in engineering and the sciences. For the analysis of shells, the use of interpolation covers to enhance solutions is presented and the new MITC3+ shell element is discussed. For transient dynamic solutions, insights in implicit and explicit time integration methods and the solution of large eigenvalue problems are given. For multi-physics analyses, the full coupling between solid, fluid, electromagnetic and thermal effects is considered. Finally, we briefly also focus on the finite element modelling of Protein and DNA nano-scale structures by coarse graining, which represents a very important frontier for future research.

Keywords: Finite element methods, shells, MITC elements, transient dynamics, explicit and implicit methods, large eigenvalue problems, modelling of proteins and DNA structures

1 Introduction

Finite element procedures have been extensively researched and developed during the last decades and are nowadays applied routinely in engineering and the sciences [1]. However, research to improve the currently available methods is continuing and very valuable advances are continuously achieved. These advances aim to establish more effective techniques for problems that can already be solved and novel techniques to be able to simulate wider ranges of physical events. The advances also pertain to applying finite element methods ingeniously to new areas of simulations. Furthermore, there are important advances that make the use of finite element procedures easier in practical analyses.

The research for more effective techniques is driven by the desire to model physical problems more accurately, using novel approaches or just finer meshes leading to an increasing number of equations to be solved. Ideally, novel techniques become available and we present in this paper new developments for the more effective analysis of shells and dynamic problems.

The simulation of wider ranges of physical problems means primarily the analysis of more complex nonlinear and multi-physics events. Here the solution of structures, in steady state or dynamic situations, with fluid-structure interactions, thermal effects, and electro-magnetic effects is of great interest. We shall briefly present our developments in these areas.

Two new areas of valuable applications of finite element methods are the coarse graining and modelling of proteins and DNA structures. The modelling of proteins is of great interest to understand their general mechanical behaviours, for example, to be able to identify changes due to disease. The modelling of DNA structures is pursued, for example, to build new devices for harvesting energy. We present below some research results in these two areas.

To make the use of finite element methods evermore easy for non-specialists is also a most important endeavor. The aim is here to reduce the amount of effort needed to build a finite element model. Fundamental advances in discretization methods, like the use of mesh-free techniques, have been made with some success but the techniques have not yet reached the required reliability and effectiveness for general applications.

Of course, the more easy use of finite element methods is an aim of great interest to industry, where the easier use is also accomplished by establishing more effective and more easy-to-use graphical user interfaces. The development of these interfaces is of major importance, but an area that we shall not comment upon.

This paper builds on two survey papers earlier written [2, 3]. In these earlier papers, we pointed out that the strategic aim, or philosophy, of a research group in its work is important. Our aim – as pursued for many years now – is to focus on the development of methods that are general, reliable and efficient, and advance the frontiers of simulations as practiced in engineering and the sciences [4]. Our experience is that with the general keen interest to solve increasingly more complex and difficult physical problems in practice, such analysis procedures are quickly adopted in applications and our aim is to make a contribution in that regard.

While these are our research aims on which we will focus in this paper, it is clear that, however, considering the complete research and development scene, as advanced by numerous researchers, many achievements published in widely available journals and books and not mentioned in this paper are also very exciting and very valuable.

In the following sections we review the latest developments in our research, with figures largely taken from our earlier papers. We refer almost only to our books and papers that however give numerous references to related accomplishments.

2 Frontiers in the analysis of shells

The analysis of shells has been pursued for decades and yet there are still important improvements needed in the effectiveness of shell elements. In practice, low-order elements are much preferred because of their ease of use in meshing, their robustness and computational efficiency, but a significant drawback is the rather low accuracy in the calculated stresses. The stress predictions can be improved by the 'stress improvement scheme' published by Payen and Bathe [5] and by the 'interpolation cover scheme' presented by Kim and Bathe [6, 7]. Both schemes were originally developed for the analysis of solids. In the following, we present the development of the interpolation cover scheme for a 3-node shell element, to obtain an enriched formulation [8], and we present a new more powerful 3-node shell element, the MITC3+ element [9]. Since this element formulation is based on the MITC technique, the extension to nonlinear analyses is directly achieved [10].

2.1 The use of interpolation covers for the MITC3 shell element

The geometry of the 3-node continuum mechanics based triangular shell finite element is interpolated using [4,11]

$$\mathbf{x}(r,s,t) = \sum_{i=1}^{3} h_i(r,s)\mathbf{x}_i + \sum_{i=1}^{3} \frac{t}{2} a_i h_i(r,s)\mathbf{V}_n^i \quad \text{with } h_1 = r,\ h_2 = s,\ h_3 = 1-r-s \quad (1)$$

where r, s, and t are the isoparametric coordinates, h_i is the interpolation function corresponding to node i, $\mathbf{x}_i$ is the position vector of node i in the global Cartesian coordinate system, and a_i, $\mathbf{V}_n^i$ denote the shell thickness and the director vector at node i, respectively.

The standard displacement interpolation of the shell element is given by

$$\overline{\mathbf{u}} = \sum_{i=1}^{3} h_i \overline{\mathbf{u}}_i + \sum_{i=1}^{3} \frac{t}{2} a_i h_i \left(-\mathbf{V}_2^i \overline{\alpha}_i + \mathbf{V}_1^i \overline{\beta}_i \right) \quad (2)$$

in which $\overline{\mathbf{u}}_i = [\ \overline{u}_i \quad \overline{v}_i \quad \overline{w}_i\ ]^T$ is the nodal displacement vector in the global Cartesian coordinate system, $\mathbf{V}_1^i = [\ V_{1x}^i \quad V_{1y}^i \quad V_{1z}^i\ ]^T$ and $\mathbf{V}_2^i = [\ V_{2x}^i \quad V_{2y}^i \quad V_{2z}^i\ ]^T$ are unit vectors orthogonal to $\mathbf{V}_n^i$ and to each other, and $\overline{\alpha}_i$ and $\overline{\beta}_i$ are the rotations of the director vector $\mathbf{V}_n^i$ about $\mathbf{V}_1^i$ and $\mathbf{V}_2^i$ at node i.

To enrich the displacement interpolation in Equation (2), we use a linear interpolation cover over the elements attached to node i [6, 7, 8]. The enriched displacement interpolation for the 3-node triangular shell finite element is given by

$$\mathbf{u} = \overline{\mathbf{u}} + \hat{\mathbf{u}} \tag{3}$$

with

$$\hat{\mathbf{u}} = \sum_{i=1}^{3} \mathbf{H}_i \hat{\mathbf{u}}_i + \sum_{i=1}^{3} \frac{t}{2} a_i \mathbf{H}_i \left(-\mathbf{D}_2^i \hat{\boldsymbol{\alpha}}_i + \mathbf{D}_1^i \hat{\boldsymbol{\beta}}_i \right) \tag{4}$$

in which $\hat{\mathbf{u}}_i = [\ \hat{u}_i^{\xi} \quad \hat{u}_i^{\eta} \ |\ \hat{v}_i^{\xi} \quad \hat{v}_i^{\eta} \ |\ \hat{w}_i^{\xi} \quad \hat{w}_i^{\eta}\ ]^T$, $\hat{\boldsymbol{\alpha}}_i = [\ \hat{\alpha}_i^{\xi} \quad \hat{\alpha}_i^{\eta}\ ]^T$ and $\hat{\boldsymbol{\beta}}_i = [\ \hat{\beta}_i^{\xi} \quad \hat{\beta}_i^{\eta}\ ]^T$ are unknown coefficient vectors for the displacements and rotations, and $\mathbf{H}_i$ is the linear cover interpolation matrix for the displacements and rotations

$$\mathbf{H}_i = h_i \begin{bmatrix} \xi_i & \eta_i & 0 & 0 & 0 & 0 \\ 0 & 0 & \xi_i & \eta_i & 0 & 0 \\ 0 & 0 & 0 & 0 & \xi_i & \eta_i \end{bmatrix},\ \mathbf{D}_1^i = \begin{bmatrix} V_{1x}^i & 0 \\ 0 & V_{1x}^i \\ V_{1y}^i & 0 \\ 0 & V_{1y}^i \\ V_{1z}^i & 0 \\ 0 & V_{1z}^i \end{bmatrix}, \text{ and } \mathbf{D}_2^i = \begin{bmatrix} V_{2x}^i & 0 \\ 0 & V_{2x}^i \\ V_{2y}^i & 0 \\ 0 & V_{2y}^i \\ V_{2z}^i & 0 \\ 0 & V_{2z}^i \end{bmatrix} \tag{5}$$

Here we employ the somewhat unusual notation that ξ_i and η_i denote coordinates in the plane of the element measured from the node i.

The covariant strain components are directly obtained by

$$e_{ij} = \frac{1}{2}\left(\mathbf{g}_i \cdot \mathbf{u}_{,j} + \mathbf{g}_j \cdot \mathbf{u}_{,i} \right) \tag{6}$$

where $\mathbf{g}_i = \dfrac{\partial \mathbf{x}}{\partial r_i}$, $\mathbf{u}_{,i} = \dfrac{\partial \mathbf{u}}{\partial r_i} = \dfrac{\partial (\overline{\mathbf{u}} + \hat{\mathbf{u}})}{\partial r_i}$ with $r_1 = r$, $r_2 = s$, $r_3 = t$

Therefore, the enriched covariant strain components are also divided into two parts

$$e_{ij} = \overline{e}_{ij} + \hat{e}_{ij} \quad \text{with } \overline{e}_{ij} = \frac{1}{2}\left(\mathbf{g}_i \cdot \overline{\mathbf{u}}_{,j} + \mathbf{g}_j \cdot \overline{\mathbf{u}}_{,i} \right) \text{ and } \hat{e}_{ij} = \frac{1}{2}\left(\mathbf{g}_i \cdot \hat{\mathbf{u}}_{,j} + \mathbf{g}_j \cdot \hat{\mathbf{u}}_{,i} \right) \tag{7}$$

in which the $\overline{e}_{ij}$ and $\hat{e}_{ij}$ correspond to the standard linear and additional quadratic displacement interpolations, respectively.

To alleviate the locking phenomenon, we use the MITC procedure but different assumed covariant transverse shear strain fields need to be employed for the standard and additional quadratic displacement interpolations. The assumed covariant transverse shear strain fields of the MITC3 and MITC6 shell elements are used for the strains $\overline{e}_{ij}$ and $\hat{e}_{ij}$, respectively [11].

The final assumed covariant transverse shear strain field for the enriched MITC3 shell element is given as

$$e_{jt}^{AS} = \overline{e}_{jt}^{AS} + \hat{e}_{jt}^{AS} = \mathbf{B}_{jt}^{AS}\mathbf{U} \quad \text{with } j = r, s \tag{8}$$

in which $\mathbf{B}_{jt}^{AS}$ is the covariant transverse shear strain-displacement matrix and $\mathbf{U}$ is the vector that contains the degrees of freedom $\overline{\mathbf{u}}_i$, $\overline{\alpha}_i$, $\overline{\beta}_i$ and the additional degrees of freedom $\hat{\mathbf{u}}_i$, $\hat{\boldsymbol{\alpha}}_i$, $\hat{\boldsymbol{\beta}}_i$.

The element matrices can now be constructed in the standard manner [4], and of course, without the cover interpolation enrichment, the element is identical to the original MITC3 shell element. With this solution approach, the covers need only be applied in certain regions of the analysis domain.

The enriched MITC3 shell element passes the membrane, bending, and transverse shearing patch tests for arbitrary local enrichments, see reference [4] for the patch tests performed.

As discussed in reference [8], the enriched MITC3 shell element is quite effective computationally and gives good convergence in solutions. Figures 1 to 6 show the convergence behaviour in the analysis of the hyperboloid shell problems that represent encompassing tests [4, 12, 13]. We use the s-norm (with the error as a relative value to the very accurate solution) to measure the solution error [8]. Good convergence behaviour is observed in particular when highly distorted meshes are used.

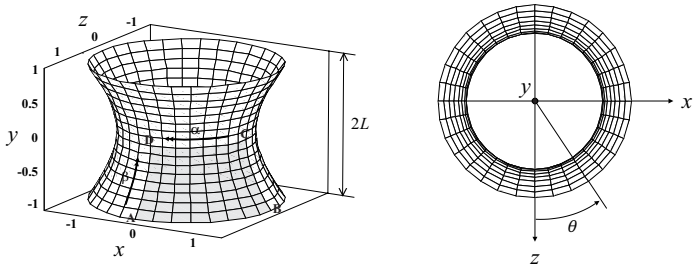

(a)

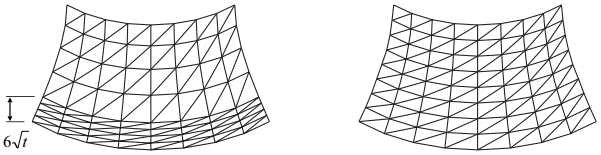

(b) **(c)**

Figure 1. Hyperboloid shell problem ($E = 2.0 \times 10^{11}$, $v = 1/3$ and $\mathrm{p}(\theta) = \cos(2\theta)$). (a) Shell geometry; only shaded part is meshed, (b) Graded mesh for the clamped case (8×8 mesh, $t/L = 1/1000$), (c) Mesh for the free case (8×8 mesh).

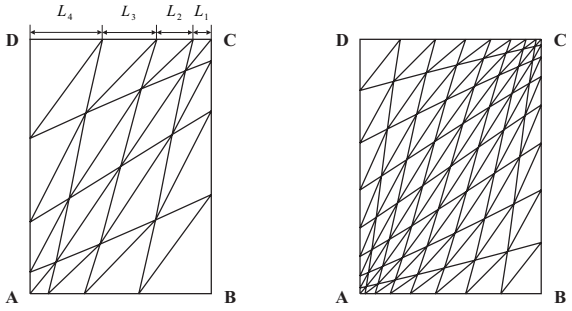

(a) **(b)**

Figure 2. Distorted meshes used when (a) $N = 4$ and (b) $N = 8$. The number of triangular elements for an $N \times N$ mesh is $2N^2$.

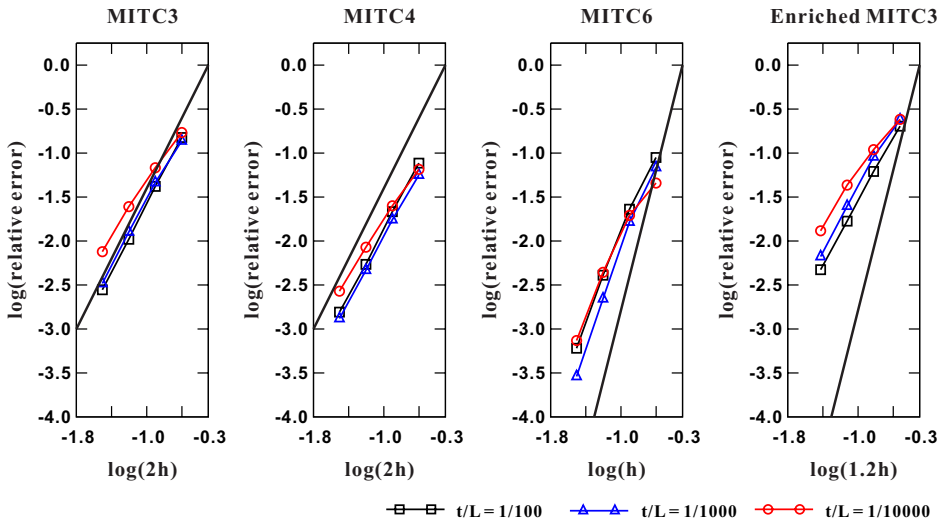

Figure 3. Convergence curves for the clamped hyperboloid shell problem with uniform meshes. The bold line represents the optimal convergence rate, which is 2.0 for linear elements and 4.0 for quadratic elements.

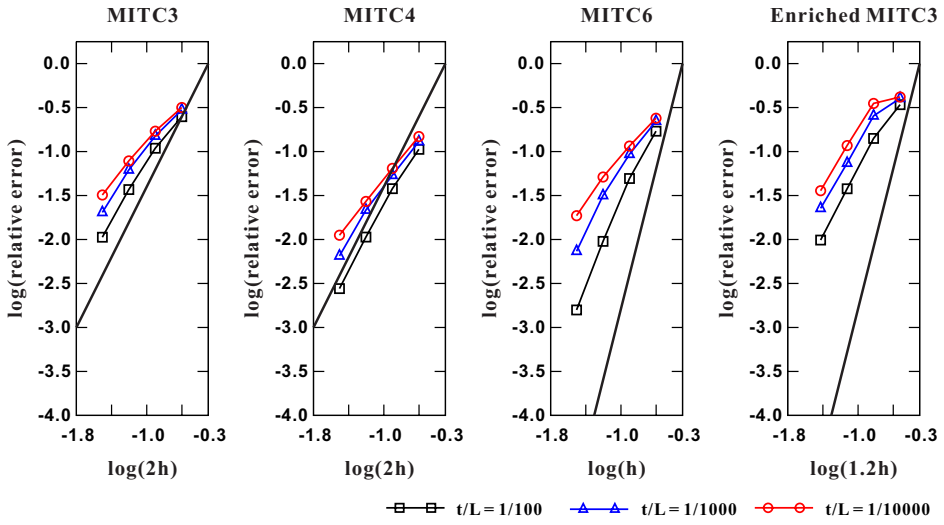

Figure 4. Convergence curves for the clamped hyperboloid shell problem with the distorted meshes shown in Figure 2

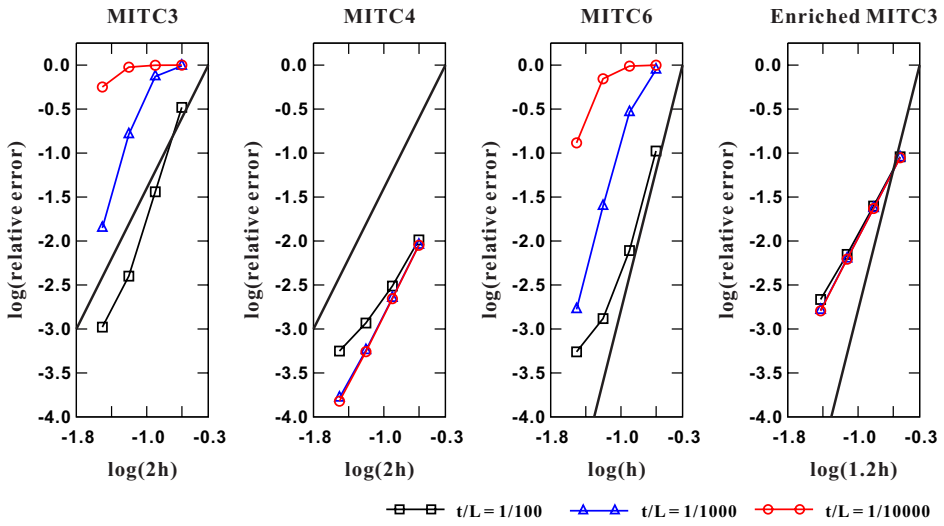

Figure 5. Convergence curves for the free hyperboloid shell problem with uniform meshes

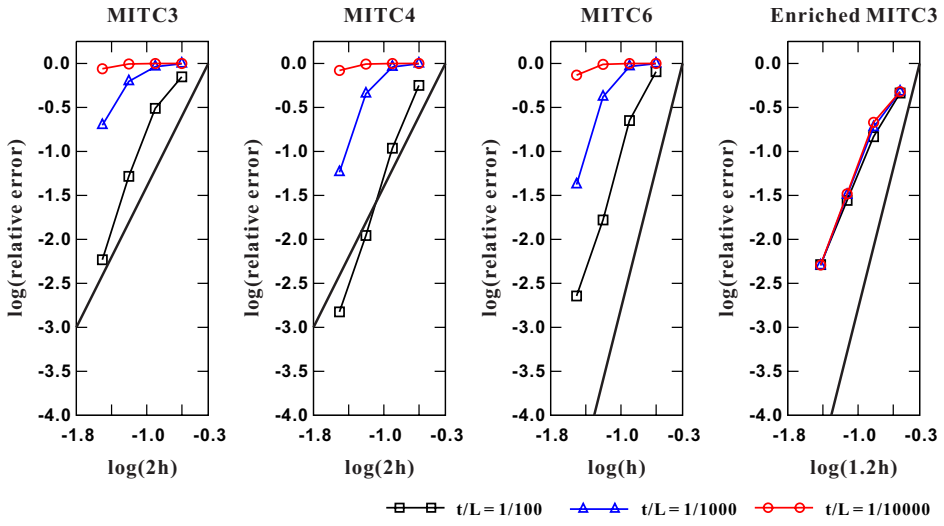

Figure 6. Convergence curves for the free hyperboloid shell problem with the distorted meshes shown in Figure 2

An important use of the 'cover interpolation scheme' is that covers need only be applied for certain nodes and elements; hence, for example, only in regions of high stress gradients. The example in Figures 7 and 8 illustrates this point [8]. More solutions showing the capabilities of the enriched MITC3 shell element are given in reference [8].

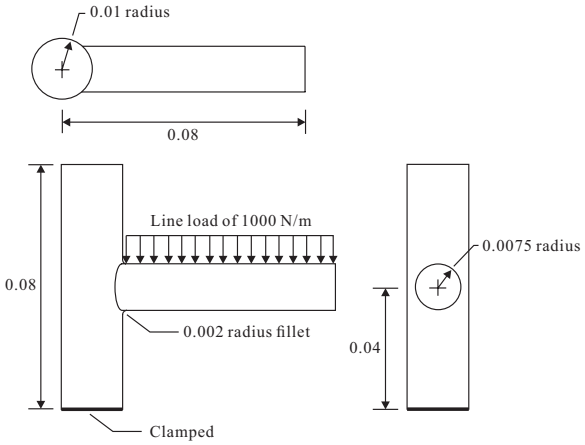

Figure 7. Shaft-shaft interaction problem with fillets ($E = 2.07 \times 10^{11}$, $\nu = 0.29$)

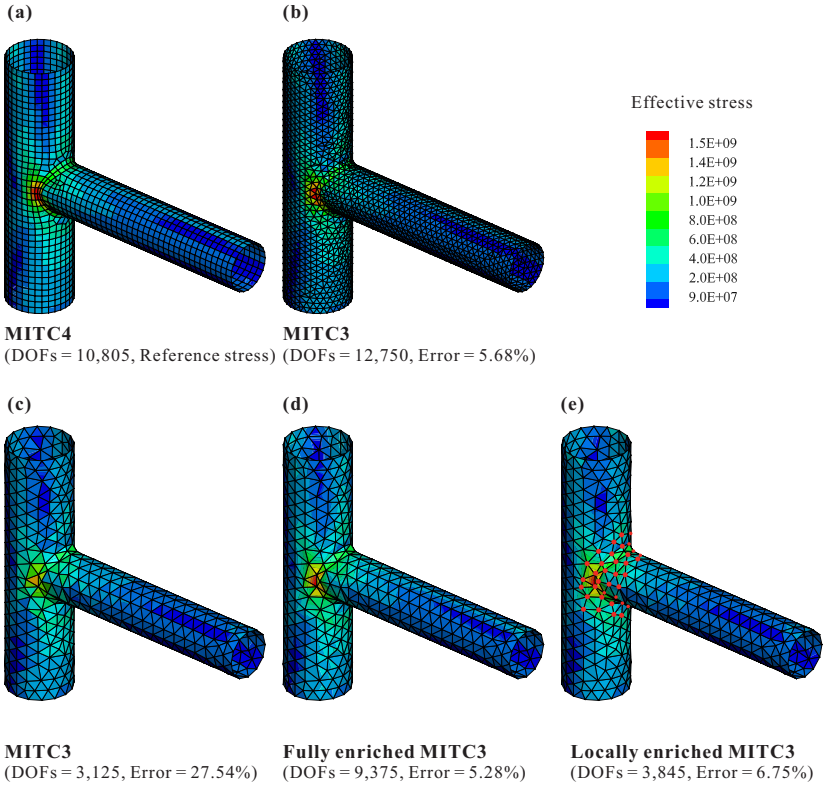

Figure 8. Effective stress for the shaft-shaft interaction problem: (a) 2,193 node model, (b) 2,582 node model, (c) 641 node model, (d) 641 node model fully enriched, and (e) the 641 node model locally enriched, where the red dots represent enriched nodes. DOFs: total number of degrees of freedom used, Error = $((\sigma_v^{ref} - \sigma_v^h)/\sigma_v^{ref}) \times 100$ with σ_v^h and σ_v^{ref} denoting the calculated and reference von Mises stresses.

2.2 A new 3-node shell element, the MITC3+ element

While the MITC3 shell element enriched by the interpolation covers is quite effective, a major challenge is to obtain a more powerful general 3-node shell element without the use of the interpolation cover scheme. In the following, we review the MITC3+ element formulation, which we developed with that important objective in mind [9, 10].

The element is based on using the usual three corner nodes and an internal forth node for a cubic bubble that however is only used to enrich the interpolation of the section rotations. The geometry interpolation of the MITC3+ shell element is hence given by

$$\mathbf{x}(r,s,t)=\sum_{i=1}^{3}h_i(r,s)\mathbf{x}_i+\sum_{i=1}^{4}\frac{t}{2}a_i f_i(r,s)\mathbf{V}_n^i \quad \text{with } a_4\mathbf{V}_n^4=\frac{1}{3}(a_1\mathbf{V}_n^1+a_2\mathbf{V}_n^2+a_3\mathbf{V}_n^3) \tag{9}$$

in which the $f_i(r,s)$ are two-dimensional interpolation functions that include the cubic bubble function f_4 corresponding to the internal node

$$f_1=h_1-\frac{1}{3}f_4,\quad f_2=h_2-\frac{1}{3}f_4,\quad f_3=h_3-\frac{1}{3}f_4,\quad f_4=27rs(1-r-s) \tag{10}$$

The corresponding displacement interpolation is [4, 9]

$$\mathbf{u}(r,s,t)=\sum_{i=1}^{3}h_i(r,s)\mathbf{u}_i+\sum_{i=1}^{4}\frac{t}{2}a_i f_i(r,s)(-\mathbf{V}_2^i\alpha_i+\mathbf{V}_1^i\beta_i) \tag{11}$$

in which α_4 and β_4 are the rotation degrees of freedom at the bubble node.

The bubble node, with the rotation degrees of freedom only, is positioned on the flat surface of the element. Hence static condensation can be carried out effectively on the element level for the rotations α_4 and β_4, and the element is in practice a 3-node shell element.

Of course, the mixed interpolation for the transverse shear strain components must now include the effects of the bubble function, which gives zero contribution along the element edges. To achieve an effective MITC tying scheme we need to look deeper into the transverse shear strain field. Considering the MITC3 shell element [11], this field can be separated into the constant part corresponding to the transverse shearing modes and the linear part corresponding to an in-plane twisting mode

$$\tilde{e}_{rt}^{MITC3} = \tilde{e}_{rt}^{const.} + \tilde{e}_{rt}^{linear}, \quad \tilde{e}_{st}^{MITC3} = \tilde{e}_{st}^{const.} + \tilde{e}_{st}^{linear}. \tag{12}$$

A similar linear decomposition can be used for the strain components of the MITC3+ element, which shows that different tying schemes can be used for the constant and the linear parts of the new element. The details of these schemes are given in reference [9]. The difficulty in the development was to achieve that the element is isotropic, not contain any spurious zero energy mode, pass all patch tests and show good convergence behaviour.

Figures 9 to 12 give the convergence curves in the s-norm obtained in the analysis of the hyperboloid shell problems described in Figure 1, using the uniform meshes in that figure and the distorted meshes in Figure 2. The good convergence behaviour of the new element is seen. Further problem solutions are given in references [9, 10].

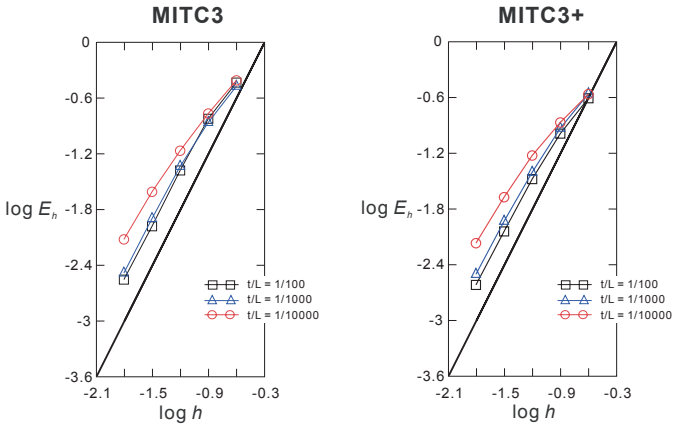

Figure 9. Convergence curves for the clamped hyperboloid shell problem with uniform meshes. The bold line represents the optimal convergence rate.

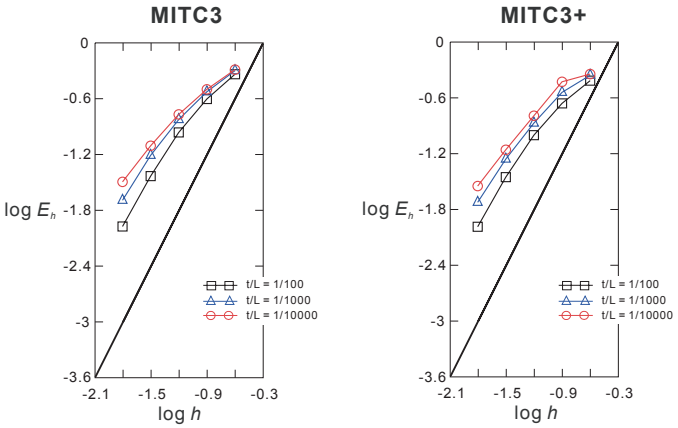

Figure 10. Convergence curves for the clamped hyperboloid shell problem with the distorted meshes shown in Figure 2

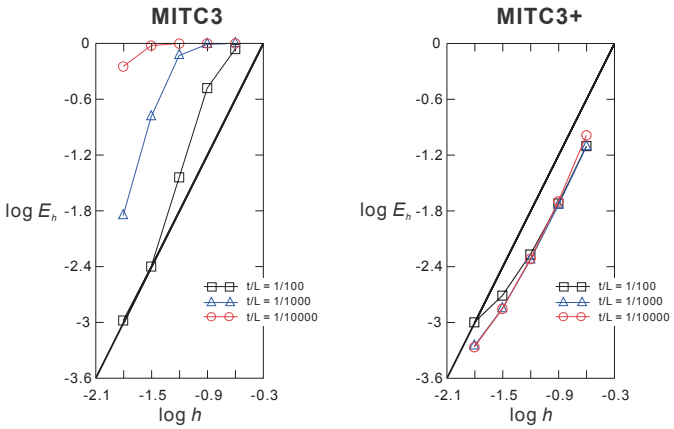

Figure 11. Convergence curves for the free hyperboloid shell problem with uniform meshes

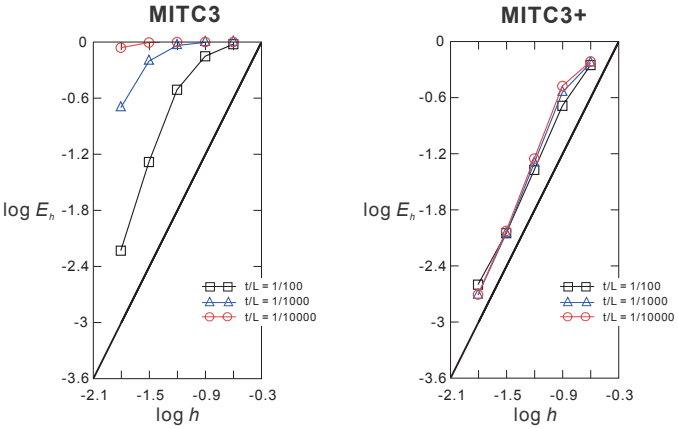

Figure 12. Convergence curves for the free hyperboloid shell problem with the distorted meshes shown in Figure 2

3 Frontiers in methods for dynamic analyses

While the development of improved solution techniques for dynamic analyses has been pursued for a long time, there is still interest in more effective techniques for nonlinear solutions, wave propagation analyses, and the solution of very large finite element models. Considering direct time integration methods, implicit time integration is frequently used and can be much preferable to explicit integration, due to the time step size restrictions and the sensitivity of the solutions to the time step size in explicit integration [4]. In the following, we briefly review an implicit scheme and an explicit scheme with new insights in the techniques, and then we consider briefly the solution of frequencies and mode shapes of very large finite element systems.

3.1 Implicit direct time integration

The implicit time integration scheme recently proposed and analysed in refs. [14-17] is increasingly employed. The technique has been presented earlier but we shall report here on some additional new insights [16,17]. The method uses two sub-steps per time step Δt. In the first sub-step, the trapezoidal rule is employed and in the second sub-step the 3-point Euler backward method is used. Of course, these two integration schemes by themselves have been employed for a long time. Considering the trapezoidal rule by itself, it is in linear analysis unconditionally stable, second order accurate, shows reasonable period elongation and no amplitude decay. However, the property of no amplitude decay can result in spurious oscillations, in linear and nonlinear analyses, and in unstable behaviour in large deformation analyses with long time durations [14,15]. Considering the Euler method by itself, it is also unconditionally stable in linear analysis, second-order accurate and shows period elongation and amplitude decay, indeed too much thereof. The proposed combination of these techniques gives an unconditionally stable, second-order accurate method that displays some amplitude decay and reasonable period elongation. In particular, this scheme does not show the undesirable characteristics of the trapezoidal rule.

Since the time step Δt is subdivided into two sub-steps of sizes $\gamma\Delta t$ and $(1-\gamma)\Delta t$, it is of interest to optimize the value of γ. With $\gamma = 2-\sqrt{2}$, the amplitude decay is maximized, the period elongation is minimized and in linear analysis the same effective stiffness matrix is used for each sub-step. Figures 13 to 15 show the excellent properties of the scheme, referred to as the Bathe method, in that the spectral radius is equal to 1 up to large time step to period ratios, the period elongation and amplitude decay show small error, but the amplitude decay increases rapidly as the time step becomes large. The figures also show that using γ = 0.5 (referred to as "Bathe") gives almost the same results as when using $\gamma = 2-\sqrt{2}$.

The consequences of these properties are that high spurious frequency response is effectively cut out of the time integration solution, while the lower frequencies are integrated very accurately. Figures 16 to 18 illustrate this behaviour in a vibration analysis. The stiff spring represents stiff components in a structural model, which may be largely due to modelling constraints with stiff elements, as frequently used in practice. The trapezoidal rule gives very large errors in this linear analysis whereas the Bathe method gives the desired response, just like obtained in a mode superposition solution only including the lowest mode response with the static correction. Further results for this problem are given in reference [16] where it is also shown that the error in the reaction R_1 is very large when using the trapezoidal rule. Finally, considering Figure 18, we note the overshoot in the prediction of the acceleration for the first time step when using the Bathe method. This overshot can be corrected by choosing different parameters in the method for this step, but that correction is probably not needed in practice.

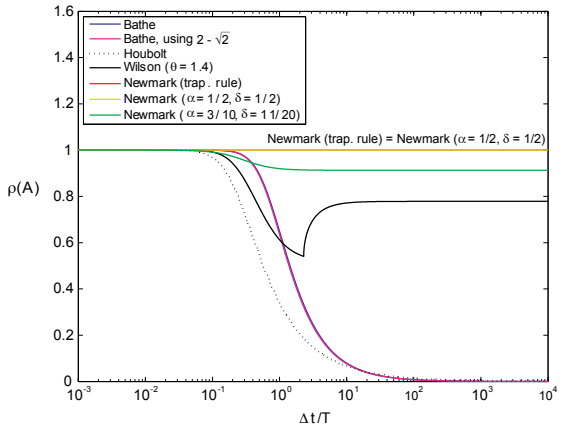

Figure 13. Spectral radii of approximation operators, case of no physical damping, for various methods

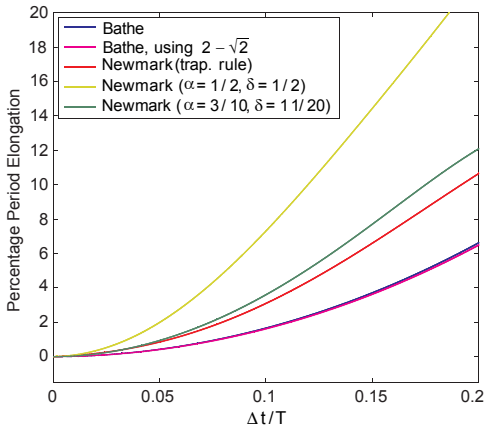

Figure 14. Percentage period elongations for various methods

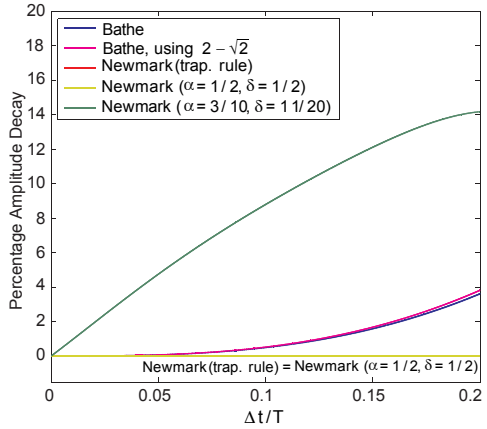

Figure 15. Percentage amplitude decays for various methods

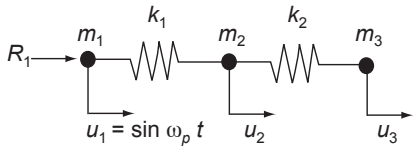

$k_1 = 10^7,\ k_2 = 1,\ m_1 = 0,\ m_2 = 1,\ m_3 = 1,\ \omega_p = 1.2$

Figure 16. Model problem of three degrees of freedom spring system

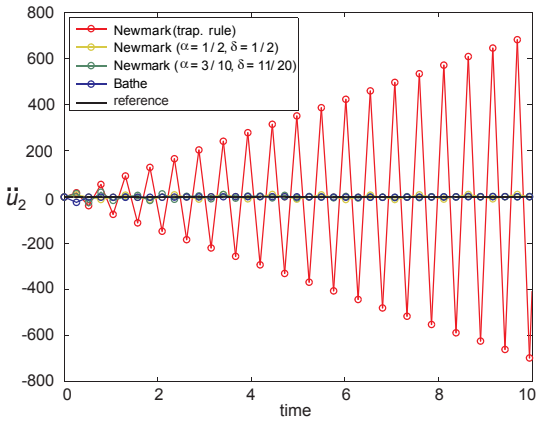

Figure 17. Acceleration of node 2 for various methods

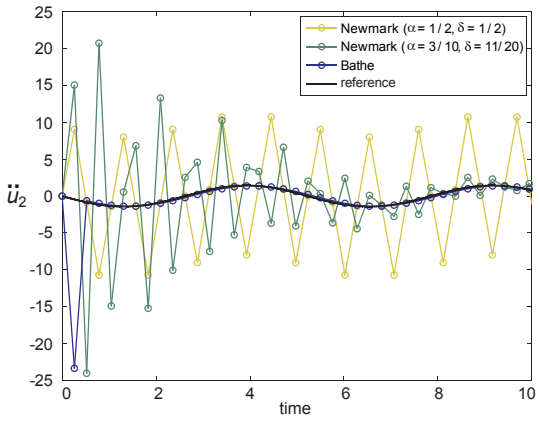

Figure 18. Close-up of acceleration of node 2 for various methods

Figures 19 and 20 give the results of an analytical study of the trapezoidal rule and the Bathe method in a wave propagation solution [17]. The figures show that the high frequency waves that cannot be resolved are simply cut out when using the Bathe method, whereas these waves remain present as errors when using the trapezoidal rule. This phenomenon is illustrated in solving the problem shown in Figure 21, see Figures 22 and 23 for the wave propagation solutions. The figures show that the Bathe method gives a significantly more accurate response prediction, and indeed using the mesh of 75×75 4-node elements with the Bathe method at its

optimal CFL = 1.0 gives a better response prediction than using the mesh of 165×165 4-node elements with the trapezoidal rule at its optimal CFL = 0.65.

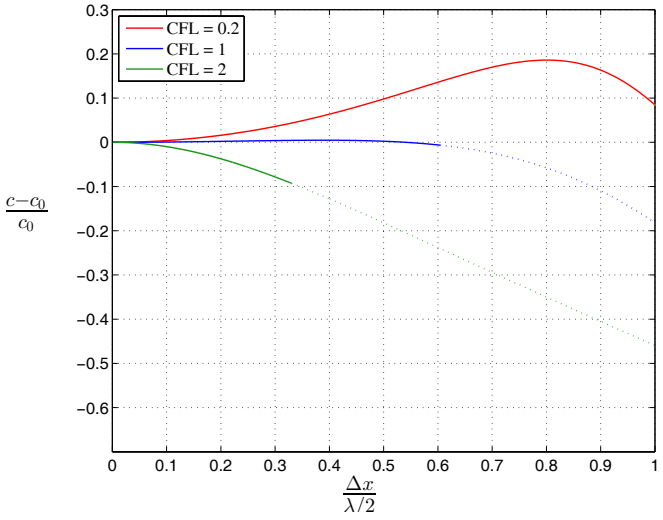

Figure 19. Relative wave speed errors of the Bathe method for various CFL numbers; results for discarded wave modes are given by dotted lines. c_0 = exact wave speed, c = numerical wave speed.

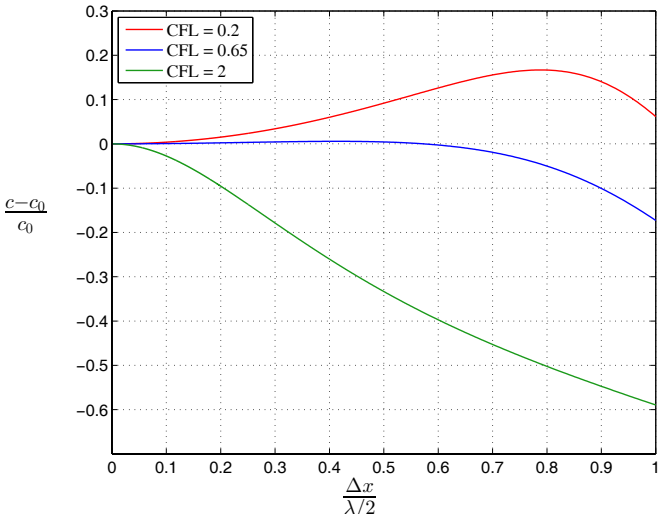

Figure 20. Relative wave speed errors of the trapezoidal rule for various CFL numbers

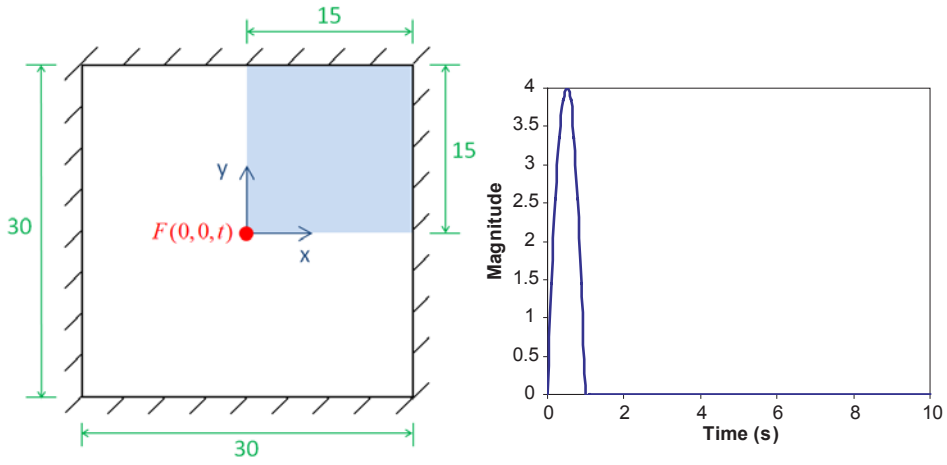

Figure 21. Pre-stressed membrane problem and load applied, $c_0 = 1$, initial displacement and velocity are zero, computational domain is shaded

Considering nonlinear analyses, the choice of an "optimal" value of γ for problem solutions is of interest. Since the Newton-Raphson iteration is used in each time step to establish equilibrium, a value resulting into fast convergence and good accuracy of the response should be used. Hence given a problem to be solved and a prescribed accuracy to be obtained in the solution, strictly, the optimal value of γ would result into the least computational effort, that is, the least number of Newton-Raphson iterations.

To illustrate the difficulties of choosing an optimal value, Figures 24 to 27 show the obtained solutions for two problems and the effect of using different values of γ on the calculated response. We see that when small time steps are employed, the use of different γ values has little effect on the calculated solution response. However, for larger time steps, there is an optimal value of γ (resulting for a given time step size into the most accurate response prediction) and this value is different for the two problems, namely it is $\gamma = 0.2$ for the problem in Figure 24 and $\gamma = 0.5$ for the problem in Figure 26. Based on these and similar studies, we are, so far, using in nonlinear analyses $\gamma = 0.5$. In this case the period elongation and amplitude decay are almost the same as for $\gamma = 2 - \sqrt{2}$ as shown in Figures 14 and 15, and good overall experience has been obtained in nonlinear solutions. In particular, our experience is that for reasonable (and almost optimal) time step sizes, of course different for the trapezoidal rule and the Bathe method, used to obtain the same solution accuracy in structural vibration problems, the total number of Newton-Raphson iterations for the complete solution can be significantly less using the Bathe method compared to when using the trapezoidal rule.

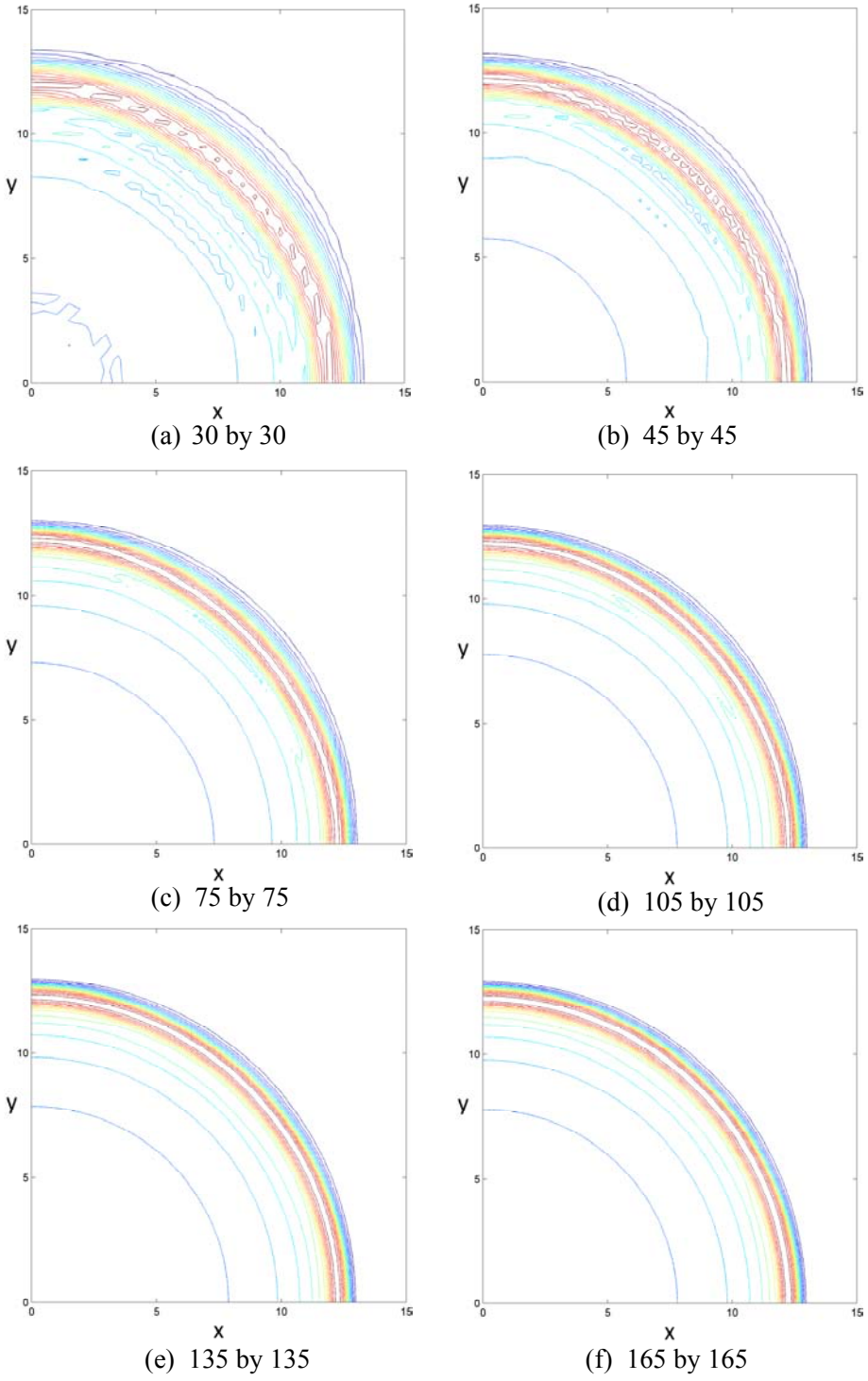

(a) 30 by 30 (b) 45 by 45

(c) 75 by 75 (d) 105 by 105

(e) 135 by 135 (f) 165 by 165

Figure 22. Snapshots of displacements at time $t = 13$, Bathe method, CFL = 1.0, using various uniform meshes

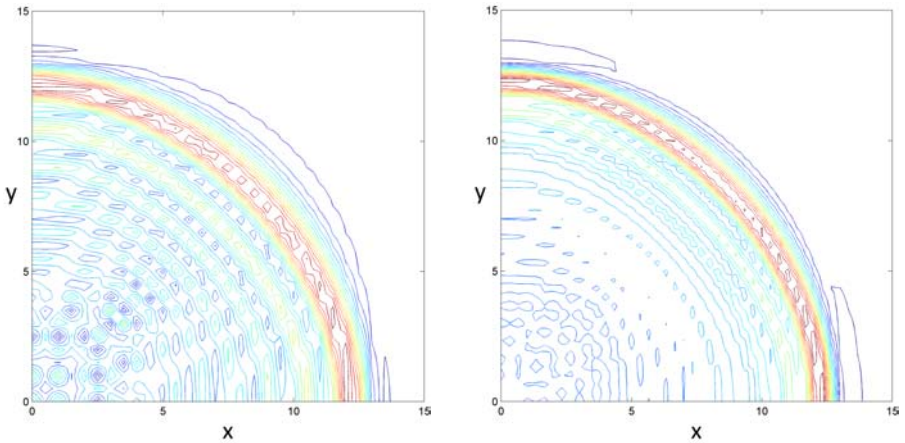

(a) 30 by 30 (b) 45 by 45

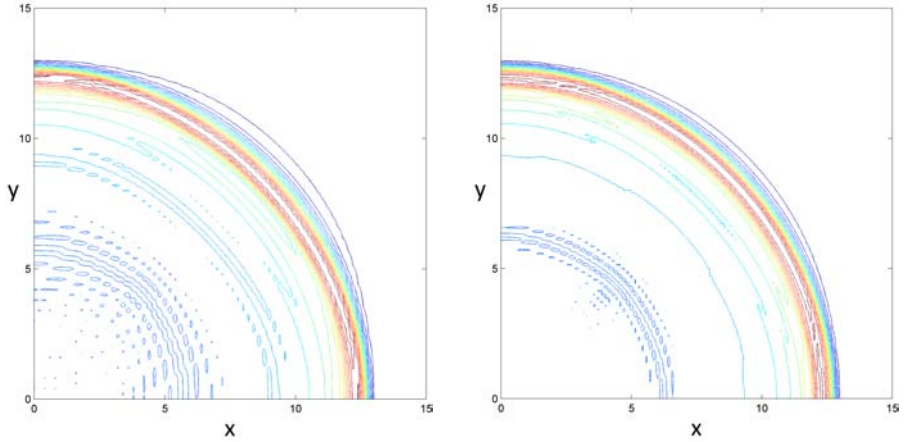

(c) 75 by 75 (d) 105 by 105

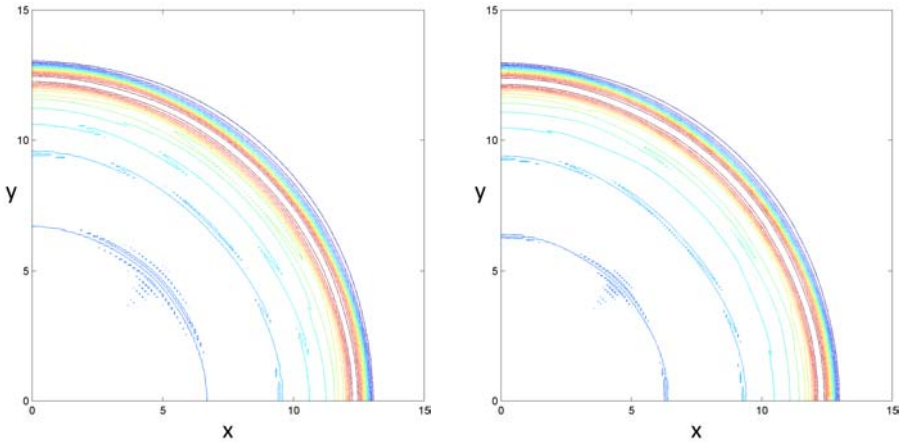

(e) 135 by 135 (f) 165 by 165

Figure 23. Snapshots of displacements at time $t = 13$, trapezoidal rule, CFL = 0.65, using various uniform meshes

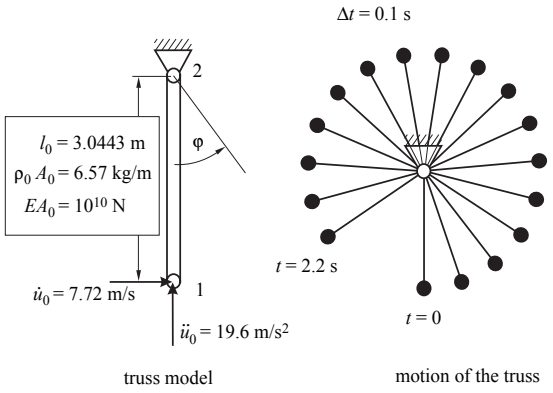

Figure 24. Simple pendulum problem solved using the Bathe method

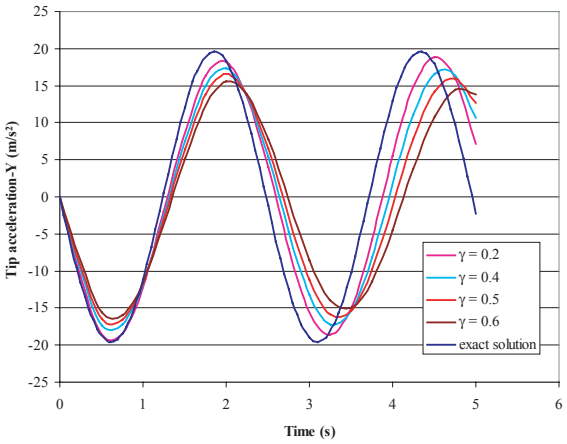

(a) $\Delta t = 0.25$s

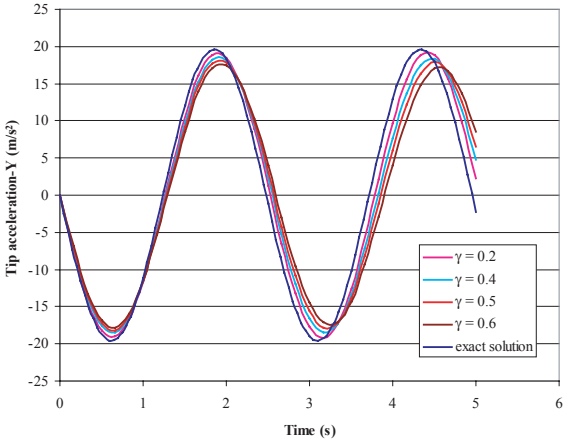

(b) $\Delta t = 0.1667$s

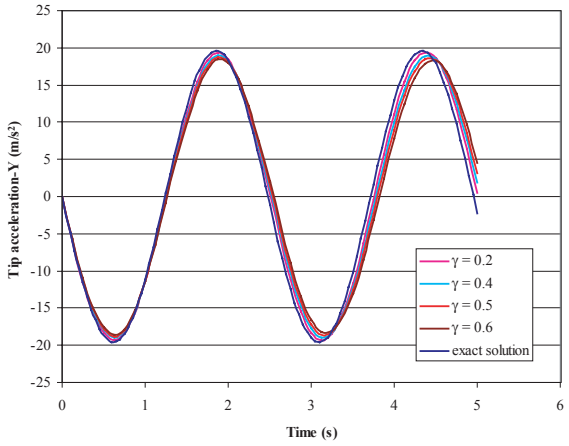

(c) $\Delta t = 0.125$s

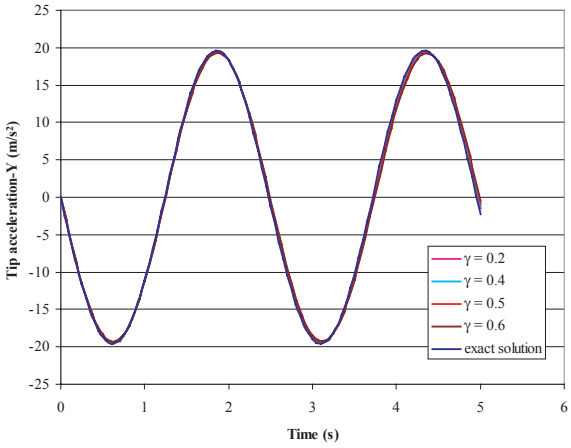

(d) $\Delta t = 0.0625$s

Figure 25. Problem of Fig. 24 solved with various values of γ and time step sizes

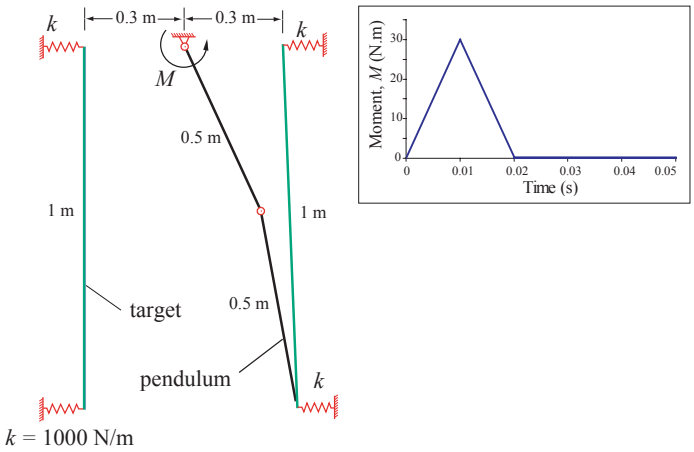

Figure 26. Double pendulum problem with contact considered using the Bathe method.

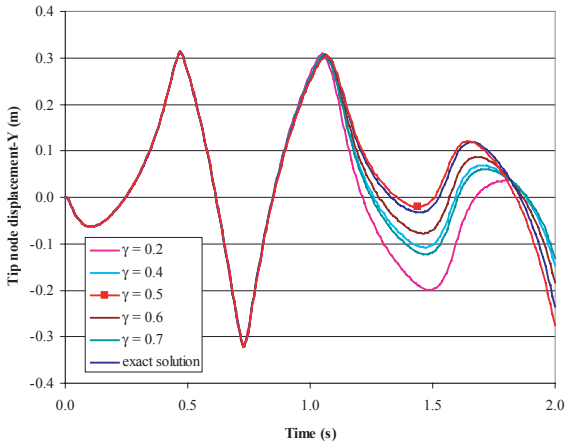

Figure 27. Problem of Fig. 26 solved with the Bathe method and various values of γ; $\Delta t = 0.005$s

3.2 Explicit direct time integration

While implicit time integration is in general preferable, explicit time integration can be more effective in the solution of certain problems, specifically in three-dimensional wave propagation solutions. Hence, we have developed a new explicit time integration scheme based on the ideas employed in the Bathe implicit scheme. In the procedure also two sub-steps are employed [18].

We use in the first sub-step

$$\mathbf{M}\,{}^{t+p\Delta t}\ddot{\mathbf{U}}+\mathbf{C}\,{}^{t+p\Delta t}\hat{\dot{\mathbf{U}}}+\mathbf{K}\,{}^{t+p\Delta t}\mathbf{U}={}^{t+p\Delta t}\hat{\mathbf{R}} \tag{13}$$

$${}^{t+p\Delta t}\mathbf{U}={}^{t}\mathbf{U}+\left[p\Delta t\right]{}^{t}\dot{\mathbf{U}}+\frac{1}{2}[p\Delta t]^2\,{}^{t}\ddot{\mathbf{U}} \tag{14}$$

$${}^{t+p\Delta t}\hat{\dot{\mathbf{U}}}={}^{t}\dot{\mathbf{U}}+\left[p\Delta t\right]{}^{t}\ddot{\mathbf{U}} \tag{15}$$

$${}^{t+p\Delta t}\dot{\mathbf{U}}={}^{t}\dot{\mathbf{U}}+\frac{1}{2}\left[p\Delta t\right]({}^{t}\ddot{\mathbf{U}}+{}^{t+p\Delta t}\ddot{\mathbf{U}}) \tag{16}$$

and in the second sub-step,

$$\mathbf{M}\,{}^{t+\Delta t}\ddot{\mathbf{U}}+\mathbf{C}\,{}^{t+\Delta t}\hat{\dot{\mathbf{U}}}+\mathbf{K}\,{}^{t+\Delta t}\mathbf{U}={}^{t+\Delta t}\mathbf{R} \tag{17}$$

$${}^{t+\Delta t}\mathbf{U}={}^{t+p\Delta t}\mathbf{U}+\left[(1-p)\Delta t\right]\,{}^{t+p\Delta t}\dot{\mathbf{U}}+\frac{1}{2}[(1-p)\Delta t]^2\,{}^{t+p\Delta t}\ddot{\mathbf{U}} \tag{18}$$

$${}^{t+\Delta t}\hat{\dot{\mathbf{U}}}={}^{t+p\Delta t}\dot{\mathbf{U}}+\left[(1-p)\Delta t\right]{}^{t+p\Delta t}\ddot{\mathbf{U}} \tag{19}$$

$${}^{t+\Delta t}\dot{\mathbf{U}}={}^{t+p\Delta t}\dot{\mathbf{U}}+\left[(1-p)\Delta t\right](q_0\,{}^{t}\ddot{\mathbf{U}}+(0.5+q_1)^{t+p\Delta t}\ddot{\mathbf{U}}+q_2\,{}^{t+\Delta t}\ddot{\mathbf{U}}) \tag{20}$$

with

$${}^{t+p\Delta t}\hat{\mathbf{R}}=(1-p)\,{}^{t}\mathbf{R}+p\,{}^{t+\Delta t}\mathbf{R} \tag{21}$$

and where q_0, q_1 *and* q_2 are a function of p, see reference [18]. A mathematical analysis of the scheme shows that p = 0.54 is good to use for stability and accuracy, with the CFL number $1/p$. Figures 28 and 29 show the spectral radius, period elongation and amplitude decay of the scheme, referred to as the Noh-Bathe method, and Figures 30 and 31 show that in a wave propagation solution, like in the Bathe implicit scheme, the high frequency waves are cut-out of the solution whereas when using the central difference method, these waves appear as solution errors. Figures 32 and 33 show the calculated response for the membrane (for the problem description see Figure 21) and we see that the Noh-Bathe method performs significantly better than the commonly used central difference scheme.

A practical solution is shown in Figures 34 and 35, where results of a crash simulation of a tube are shown. The spurious oscillations using the central difference scheme are clearly seen, and these are not present when using the Noh-Bathe procedure. In such crash and crush simulations, involving very large strains, the 3D-

shell element presented in reference [19] is valuable. Such problems can also frequently be solved quite effectively using implicit time integration [2, 20].

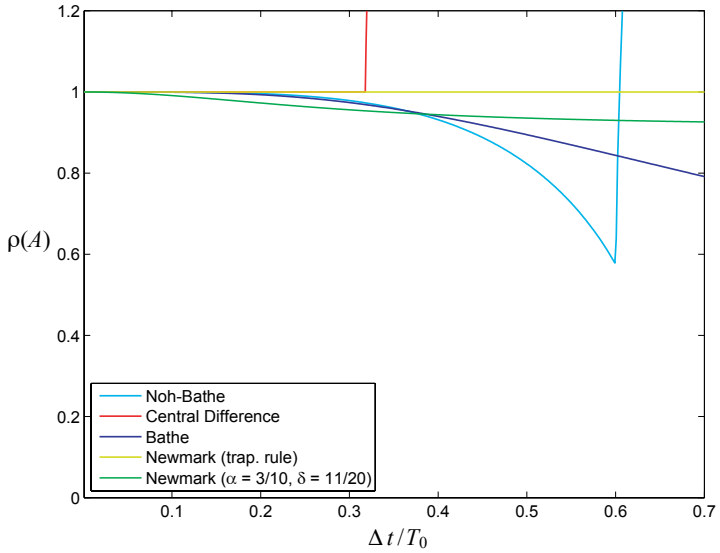

Figure 28. Spectral radii of approximation operators, case of no physical damping, for various methods; for the Noh-Bathe explicit scheme, $p = 0.54$ is used

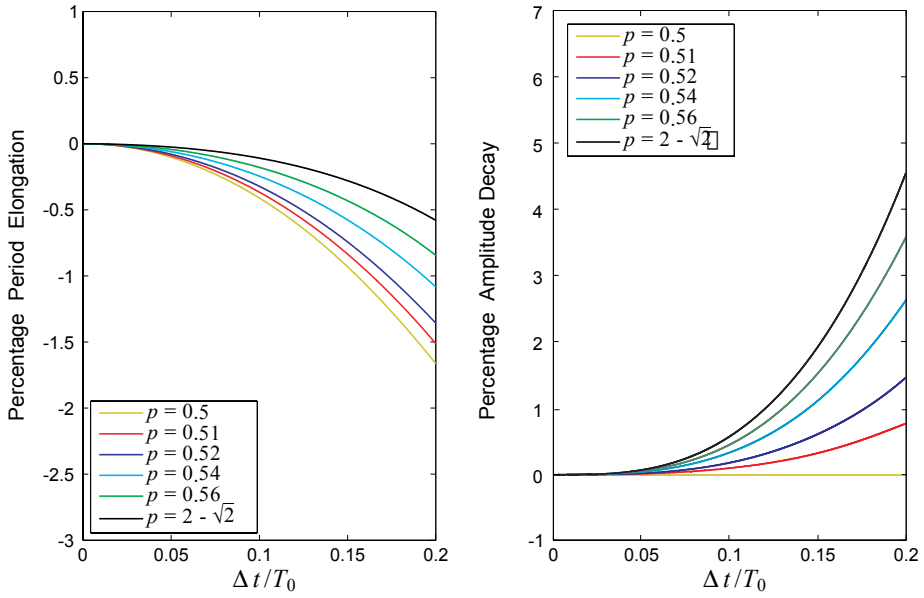

Figure 29. Percentage period elongations and amplitude decays of the Noh-Bathe scheme

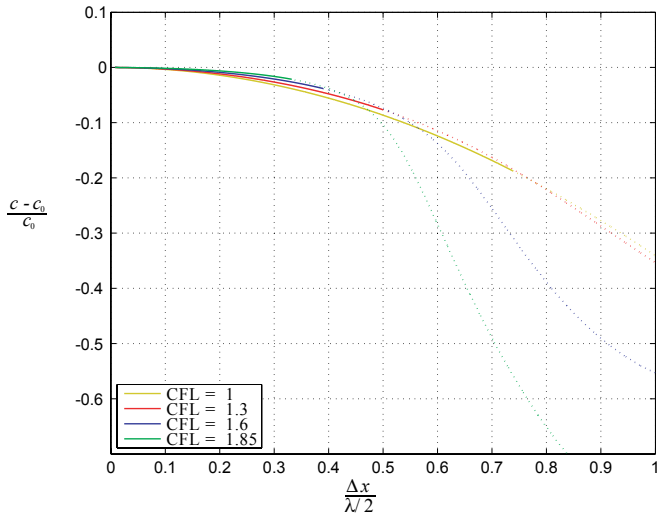

Figure 30. Relative wave speed errors of the Noh-Bathe scheme for various CFL numbers, using $p = 0.54$; results for discarded wave modes are given by dotted lines. c_0 = exact wave speed, c = numerical wave speed

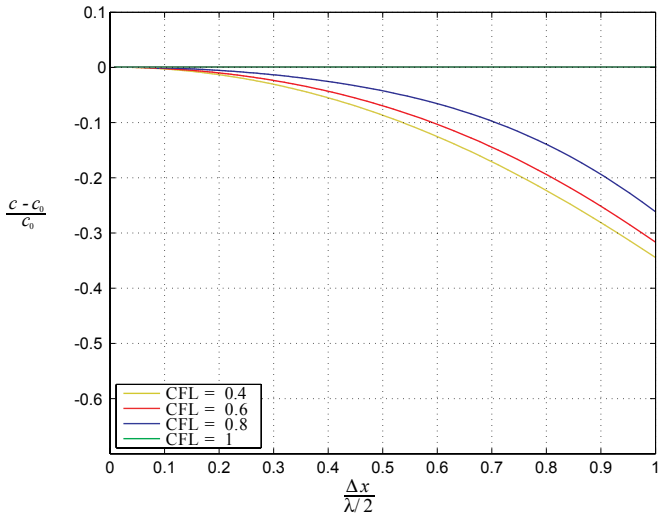

Figure 31. Relative wave speed errors of the central difference method for various CFL numbers

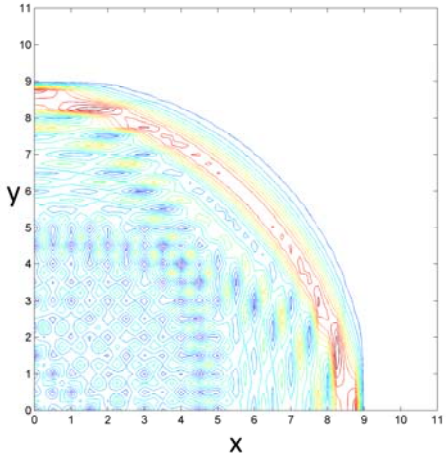

(a) 44 by 44

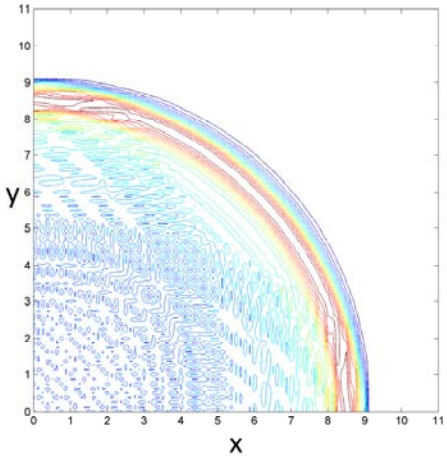

(b) 88 by 88

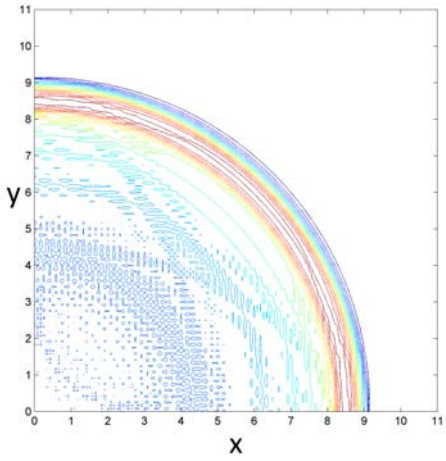

(c) 132 by 132

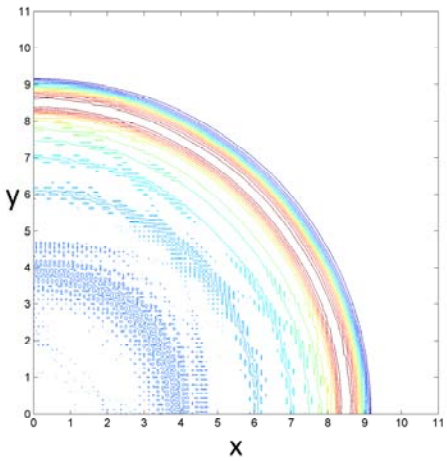

(d) 176 by 176

Figure 32. Snapshots of displacements at $t = 9.25$, central difference method, CFL = 1, uniform meshes of 4-node elements used

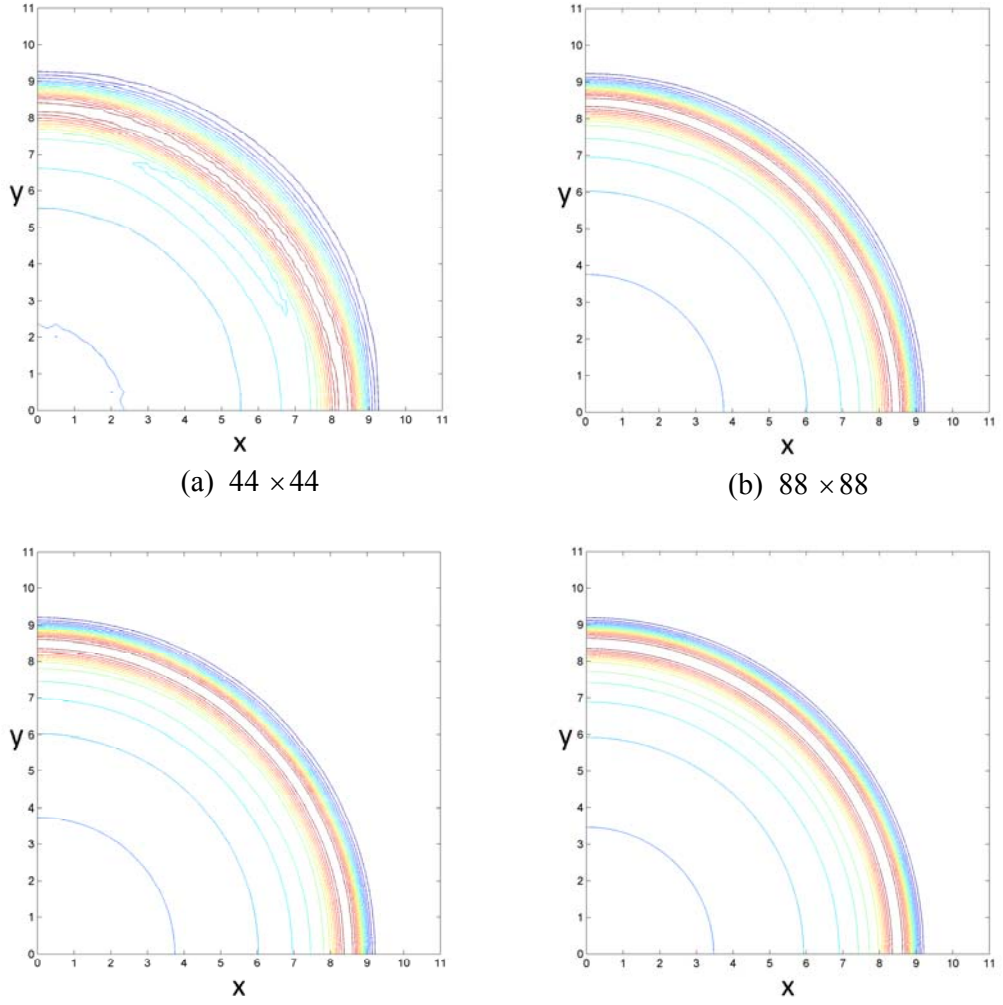

(a) 44×44 (b) 88×88

(c) 132×132 (d) 176×176

Figure 33. Snapshots of displacements at $t = 9.25$, Noh-Bathe method, CFL = 1.85, $p = 0.54$, uniform meshes of 4-node elements used

It is interesting to note that considering the response predictions in Figures 32 and 33, the Noh-Bathe method gives a more accurate response with the 44×44 mesh than when using the 176×176 mesh with the central difference method. This is an illustrative example that, as also implied by Figures 30 and 31, the meshes used in wave propagation analyses should depend more than in structural vibration problems on the specific time integration scheme employed.

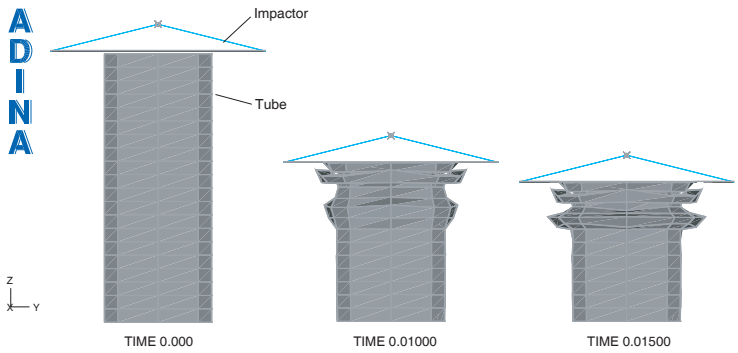

Figure 34. Tube-crush problem: Noh-Bathe method predicted deformations at t = 0.000, 0.010, and 0.015s

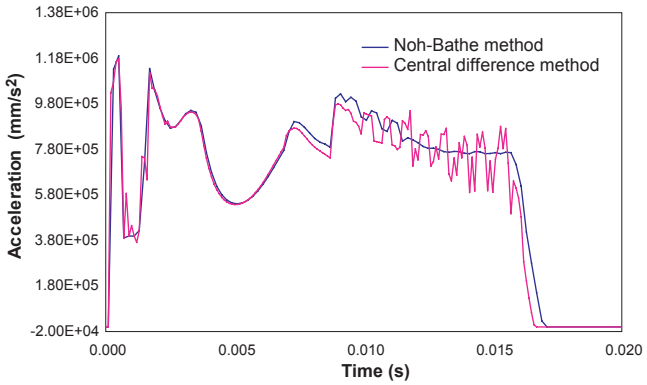

Figure 35. Impactor acceleration-time response for the tube in Figure 34

A particular advantage is that damping with a non-diagonal damping matrix can directly be included in the solution, see Equations (13) to (21). Hence the scheme can sometimes be used for large finite element systems to obtain the static solution by introducing, for example, Rayleigh damping [4].

In practical analyses it may also be of advantage to perform partly explicit and partly implicit time integration for the response solution. For example, for a short initial duration the explicit scheme may be used and then the implicit method may be more effective. Such solution is directly possible because we use the same element formulations in the different time integrations. Also, a static analysis followed by a transient dynamic analysis is directly possible, as may be required in the snap-through buckling response solution of a shell [4].

While we focused here, for dynamic analyses, on time integration schemes, it is of course also important to achieve advances in the basic spatial finite element discretizations for dynamics. We have pursued the enrichment of traditional finite elements and the method of finite spheres for dynamic analyses using harmonic functions [21, 22]. These schemes show also considerable promise.

3.3 The solution of large eigenvalue problems: using component mode synthesis with subspace iterations

The accurate solution of large eigenvalue problems, with millions of governing finite element equations and hundreds of frequencies and mode shapes to be solved for, is now quite common. The Lanczos iterative scheme and the Bathe subspace iteration method are mostly used to calculate the eigenvalues and vectors [4, 23]. However, in engineering designs and analyses of very large physical systems, like airplanes, first, the individual components (like the wings, the main body of the airplane) might be considered and optimized and then thereafter the complete physical system is also analysed in detail. In these cases a component mode synthesis solution might be used, for example the Craig-Bampton scheme or a variation thereof. The drawback of using these component mode synthesis schemes is that the error in the frequency and mode shape solutions of the complete model is hardly assessed.

A natural way to proceed is, however, to consider the component mode synthesis scheme to be a Rayleigh-Ritz analysis and then to continue with subspace iterations [23, 24]. As part thereof, proven error bounds are calculated and can be used to assess the error in the solutions [4, 24]. As an illustrative example, Figure 36 shows a pipe bend, modelled using shell elements with 258,900 degrees of freedom, for which the lowest 100 frequencies and corresponding mode shapes are required. Figure 37 shows the calculated frequencies obtained using the Craig-Bampton scheme and performing one and two additional subspace iterations. As expected, the subspace iterations greatly reduce the error in the solution and can be used to control the error. Additional results are given in reference [24].

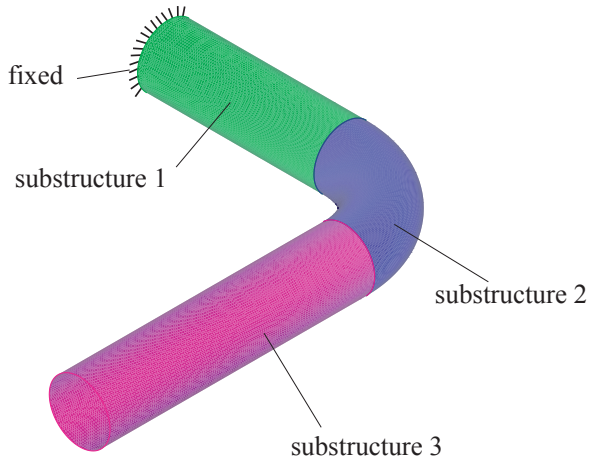

Figure 36. Pipe bend used in Craig-Bampton scheme and Bathe subspace iteration method

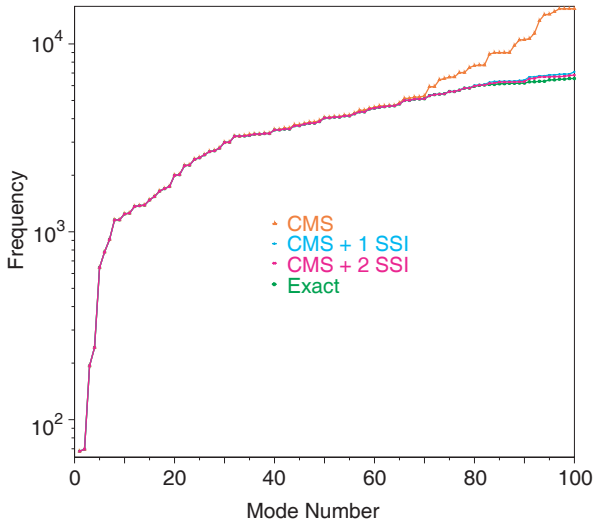

Figure 37. Calculated frequencies using the Craig-Bampton scheme and subsequent subspace iterations; use of 200 vectors

4 The solution of multi-physics structural problems including electromagnetic effects

The solution of multi-physics problems is now given increasing attention. The multi-physics effects on structures may be due to the interactions with fluids, heat flows, and electromagnetic effects. To include the electromagnetic interactions opens the possibilities to problem solutions in many new analysis areas, but is particularly difficult. Here we briefly discuss our latest developments to include electromagnetic effects in the analysis of structures and fluids.

4.1 The solution of Maxwell's equations by conservative forms

The electromagnetic effects are governed by the general Maxwell's equations that must be written in an appropriate form for finite element solutions. Since the electromagnetic effects are largely governed by expressions involving the curl operator, nodal edge-based elements are employed. However, for coupling to the commonly used fluid and structural elements, electromagnetic elements that are described by degrees of freedom at the usual corner and mid-side nodes could be much more effective.

To reach a suitable formulation, we write the fundamental first-order Maxwell's equations as second-order equations, with appropriate boundary conditions, and in conservative form [2, 25]. The second-order equation system gives suitable divergence conditions, considering Faraday's law

$$\nabla\bullet\left(\left(p+\rho_0/\varepsilon^*\right)\mathbf{I}-\nabla\mathbf{E}+\mathbf{I}\times\mathbf{K}\right)=\mathbf{0} \tag{22}$$

and the Ampere-Maxwell law

$$\nabla\bullet\left(q\mathbf{I}-\nabla\mathbf{H}-\mathbf{I}\times\mathbf{J}\right)=\mathbf{0} \tag{23}$$

where **E** and **H** are the electric and magnetic field intensities, respectively, **I** is the identity tensor, **K** is an imposed magnetic current density that includes the effect of the magnetic field **B**, where $\mathbf{B}=\mu\mathbf{H}$, **J** is an imposed electric current density that includes the Maxwell displacement current, ε^* and μ are the effective permittivity (for static and harmonic solutions) and permeability of the material in the fields, ρ_0 is a charge density source, and we introduced the solution variables

$$p=\nabla\bullet\mathbf{E}-\rho_0/\varepsilon^*;\quad q=\nabla\bullet\mathbf{H} \tag{24}$$

Equations (22) to (24) form the **E-H** mathematical formulation that we use for our finite element solution. The divergence form of the governing equations is used to directly satisfy conservation like in the FCBI formulation of fluid flows [26 - 28]. Indeed to solve these equations we employ the same weight and interpolation functions and control volumes as in the fluid flow solutions.

While the use of the **E-H** formulation can be effective, depending on the given boundary conditions, a potential formulation has advantages of less degrees of freedom and the boundary conditions are given in terms of potentials, which may be attractive. Hence we also use a potential formulation but again based on conservative forms of the governing equations [25].

4.2 Coupling of electromagnetic effects into fluid flows and structures

Using the **E-H** formulation, the Lorentz force and Joule heating rate are computed directly to couple into the structural and fluid flow response without further differentiations that are required in the potential formulation. We then establish the coupled governing equations as in fluid-structure interaction solutions [27, 28].

Consider the multi-physics analysis of water flowing through a duct in which the water is heated by a guided microwave at the frequency of 915MHz. Figure 38 shows the system schematically.

At the inlet of the fluid flow, the velocity is prescribed, varying between 0.015 m/s and 0.060 m/s, and the temperature is prescribed at 293K. At the outlet, zero pressure and zero heat flux are specified. The sides of the duct are modelled as no slip adiabatic walls.

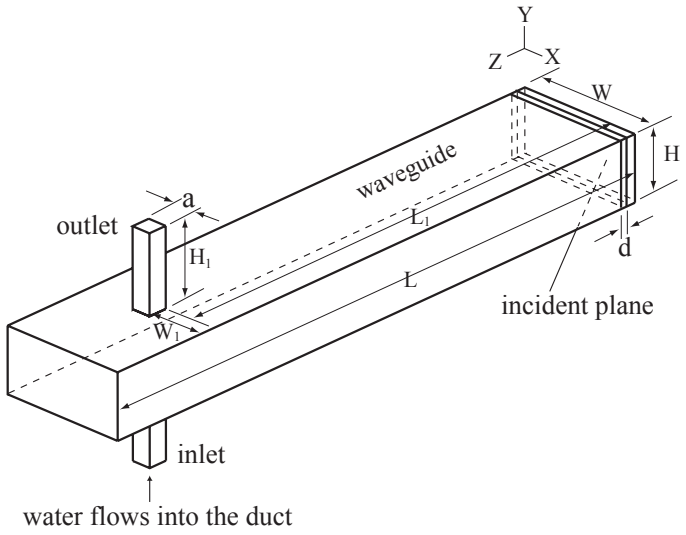

Figure 38. Schematic figure of the microwave heating system, square duct, dimensions in meters: L = 1.212, W=0.248, H=0.124, L_1= 0.99, W_1=0.105, H_1=0.15, a=0.038, d=0.0001

Figures 39 to 42 show some solution results. In particular, Figure 42 gives the averaged water temperature in the duct along the flow direction, due to the electromagnetic heating for different inlet velocities. Further details of this analysis and results, as well as other physical problem solutions are given in reference [25].

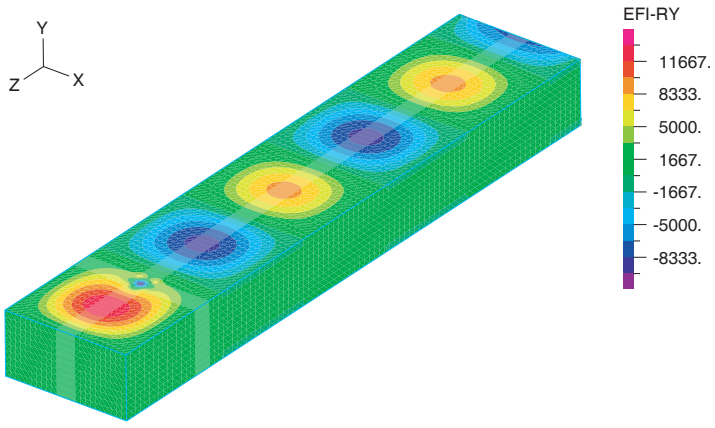

Figure 39. Calculated real Y-component of the electric field intensity

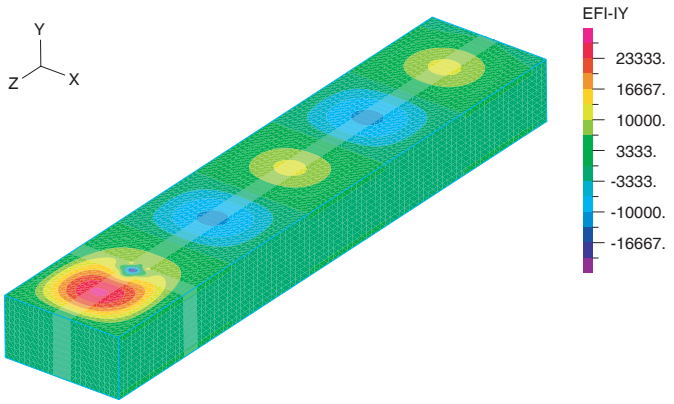

Figure 40. Calculated imaginary Y-component of the electric field intensity

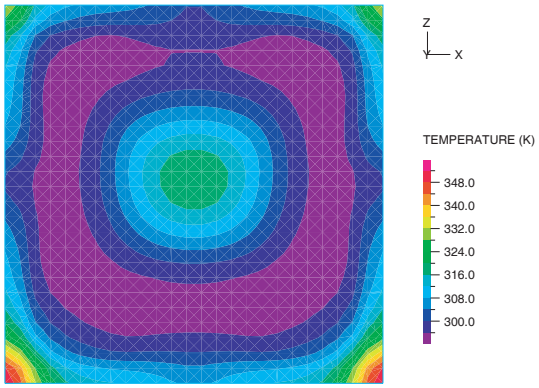

Figure 41. Temperature distribution in the cross-section of the duct at the mid-plane of the wave guide

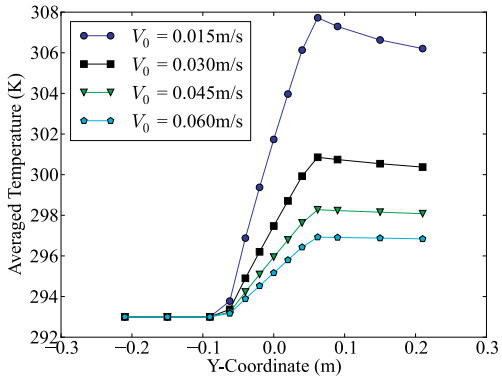

Figure 42. Averaged water temperature in the duct along flow direction for different inlet velocities V_0

5 Finite element simulations at the nano-scale: protein and DNA structures

The finite element analysis of nano-scale structures has been given significant attention, in various research areas. For example, nano-tubes have been studied in detail to understand their mechanical behaviours.

Our interest has been in the finite element simulations of proteins and DNA structures. Figure 43 gives an overview of how these structures are basic building blocks of cells, and hence of life.

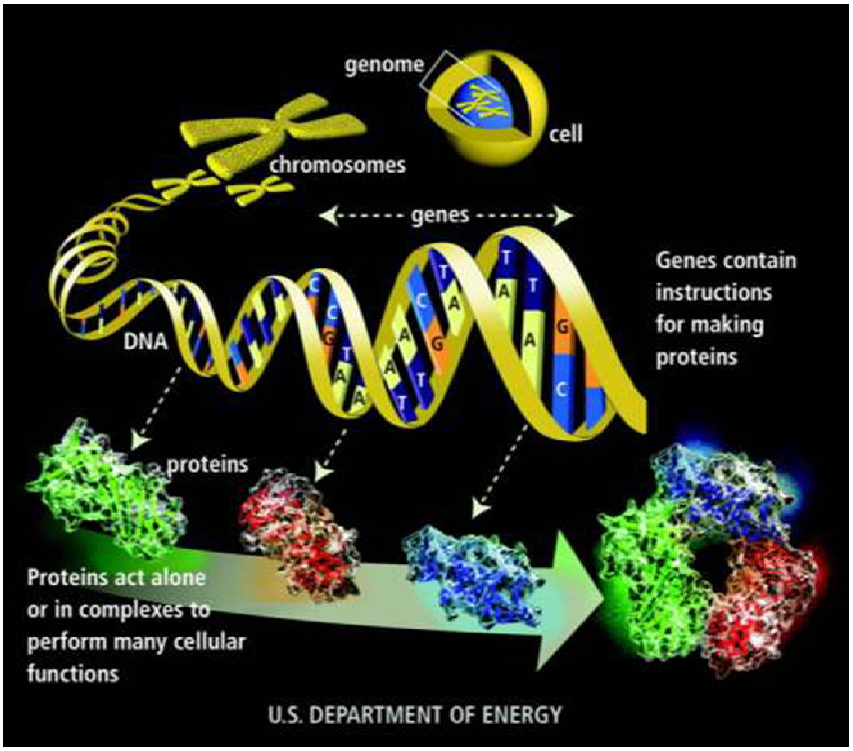

Figure 43. Overview, courtesy US Department of Energy

5.1 The simulation of proteins

Proteins have been studied for many years. The interest lies in understanding the mechanical behaviour of proteins in their various configurations, including their dynamic response. Using the results of these studies, the premise is, for example, that the malfunction of proteins and hence the development of disease can be predicted. The most basic approach is to use molecular dynamics to solve for the response of proteins. However, such simulations are extremely expensive computationally. Indeed, such studies can only be conducted on very small single

proteins using very powerful computers, whereas we are in fact interested in studying assemblages of proteins. Hence simplified models must be used to study protein behaviours.

Conceptually simple models include, for example, the elastic network model and the bead model, in which the structures of proteins are represented, in essence, by rigid bodies connected by springs. Also, the block normal mode method is used. However, recently, M. Bathe proposed the use of the finite element method as a much more general and powerful modelling procedure [29]. With the finite element discretization technique, frequencies and mode shapes not including the solvent effects can be studied, and normal mode solutions can be obtained [30]. Furthermore, the mechanical behavior of proteins including solvent effects can also be simulated using Langevin or Brownian dynamics [31].

In the finite element analysis approach, the surface of the protein is used to mesh the volume with solid elements, see Figure 44.

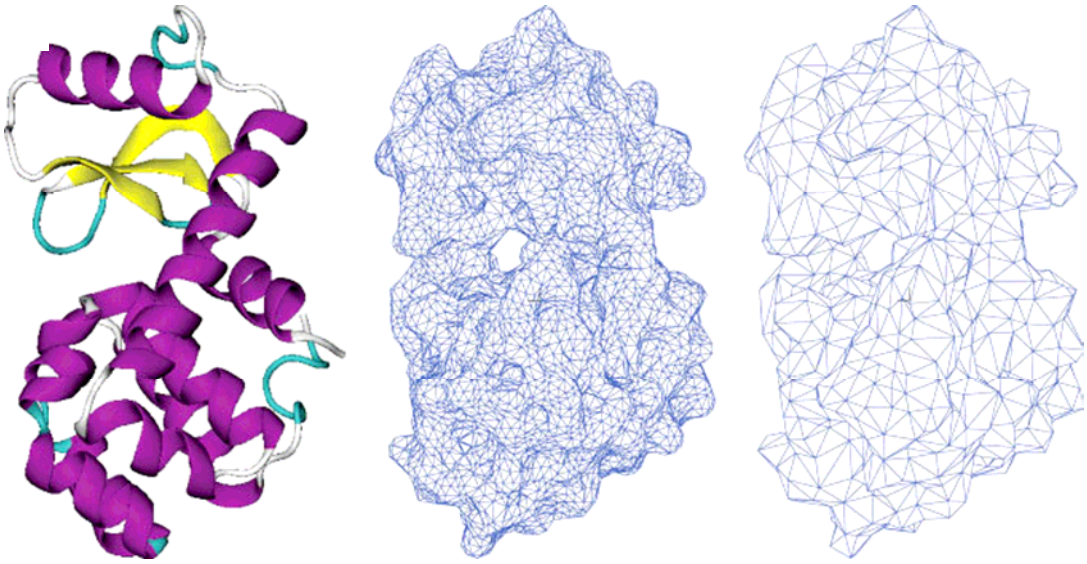

Figure 44. A protein in its fine and coarse finite element representations [29]

The governing equations of the finite element system in Langevin dynamics are

$$\mathbf{M}\ddot{\mathbf{x}} + \mathbf{Z}\dot{\mathbf{x}} + \mathbf{K}\mathbf{x} = \mathbf{f}(t) \tag{25}$$

where **M** is the mass matrix, **Z** is the friction matrix, **K** is the stiffness matrix, **f** is the solvent-induced forcing, and **x** is the vector of nodal displacements. In Brownian dynamics, the inertia effects are neglected.

The key difficulty is to establish an appropriate friction matrix. This has been accomplished in reference [31] by modelling the solvent as an incompressible Stokes fluid and establishing an influence matrix corresponding to all surface degrees of freedom of the protein model. Using the friction matrix, typical results obtained in a Brownian dynamics solution are given in Figure 45. The figure shows the root mean square fluctuations for different points of the protein.

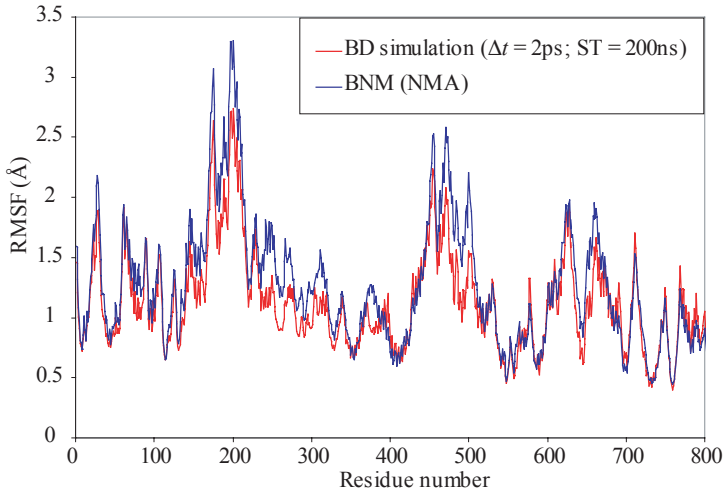

Figure 45. The protein Taq polymerase; results using finite element coarse graining with a Brownian dynamics, BD, solution compared to using the block normal mode method, BNM (NMA), not including the effect of solvent (residue number refers to a point); ST= solution time used

5.2 The simulation of DNA structures

The design and simulation of DNA structures is of great interest because these tiny structures might be fabricated to serve various purposes, like for certain functionalities in computers, for therapeutic purposes to carry medication, and in energy harvesting.

Figure 46 shows an array of DNA structures [32]. The key here is to design DNA structures from initial configurations to obtain optimal shapes for specific functionalities. The shapes need to be calculated through highly nonlinear analyses, largely using beam and alignment elements, in which buckling and ultimate load points are encountered with softening and hardening regimes [33]. Figure 47 shows a calculated DNA shape using the CanDo program [34] and a comparison with laboratory test data.

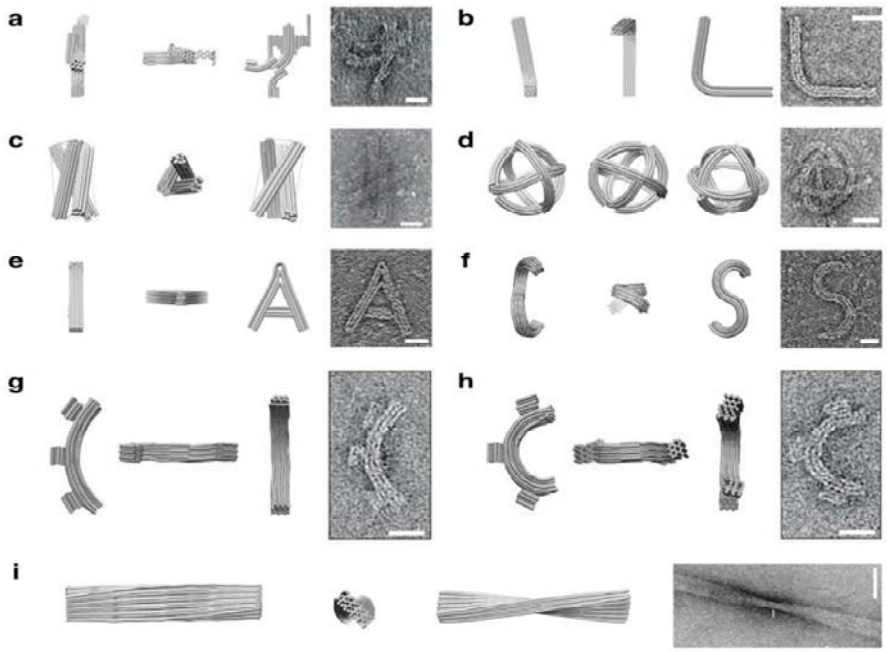

Figure 46. Various DNA structures

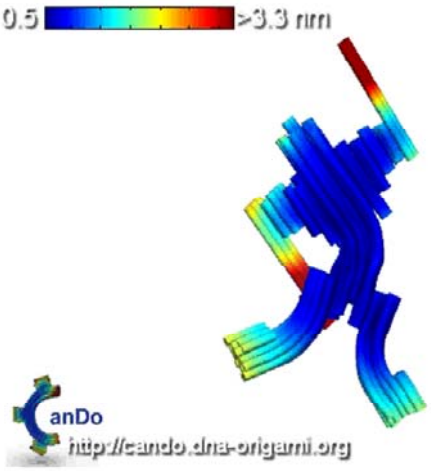

(a) Finite element simulation

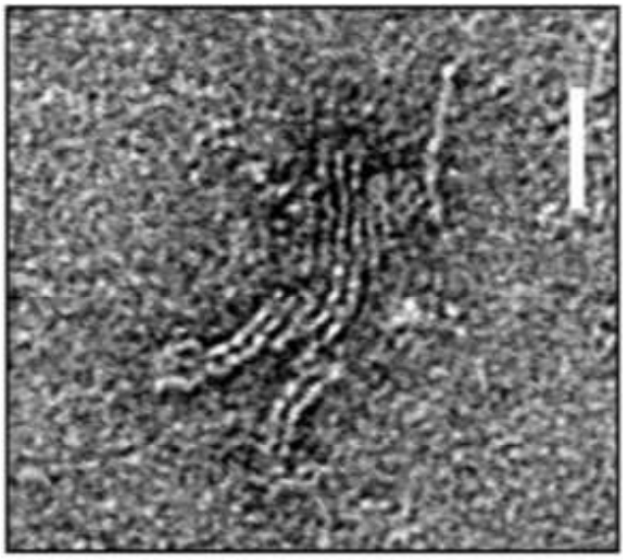

(b) Electron microscope measurements

Figure 47. A DNA finite element solution

This field of finite element analysis promises to have a very significant impact in the areas of sciences and engineering, and is still wide open for major contributions. The field requires multi-physics simulations for which novel finite element analysis schemes are needed because, for example, the analyses will involve strong coupling to chemical and electromechanical phenomena. Furthermore, in some areas, the simulations at the nano-scale will ultimately have to be coupled to models of large-scale structures in order to study the effects seen at the nano-scale on the behaviour of these structures, see Figure 43. As in practically all analyses but particularly here — an important ingredient for all these simulations is that the analyses need to be guided, as much as possible, by knowledge obtained through laboratory test data. However, the exciting part is that finite element analyses can guide the design of appropriate laboratory tests, will give crucial insights that cannot be measured and reached in these tests, and perhaps most importantly, the analyses can be used in the design of optimal DNA structures.

6 Concluding remarks

The objective in this paper was to survey some of our recent developments in frontiers of finite element procedures. In our research we focus on the development of novel finite element formulations, solution techniques, and applications.

As pointed out in the paper, we aim to establish new finite element procedures that are reliable and effective, and to obtain new insights in the properties of solution techniques through mathematical analysis and testing.

As for new procedures, there are still many important challenges for developments to enlarge the applicability of finite element methods to wider areas of analysis and to increase the effectiveness of finite element techniques, specifically for multi-physics solutions. However, new insights through analysis and testing of established and already widely-used finite element methods are also very important and should be continuously pursued, see reference [35] for an example in this respect, with some surprises in results using finite elements with incompatible modes.

The field of finite element analysis is already very large but the applications are bound to grow still very significantly, and in fact 'we might conjecture that we are now only at the beginning of the use of finite element methods'. In this continuous growth of applications, it is likely that the approach of 'hierarchical modeling' will play a significant role in all analyses, but in particular in nonlinear and multi-physics solutions [36].

Acknowledgements

I would like to acknowledge my collaboration with my many students at M.I.T. and colleagues at ADINA R & D, referred to in the references, which has resulted in the research results and developments presented herein.

References

In this survey article, we almost only refer to our publications, however, with numerous references given therein.

[1] K.J. Bathe, "The Finite Element Method", in "Encyclopedia of Computer Science and Engineering", B. Wah, (Editor), Wiley and Sons, Inc., 2009.

[2] K.J. Bathe, "Advances in the Multiphysics Analysis of Structures", Chapter 1 in "Computational Methods for Engineering Science", B.H.V. Topping, (Editor), Saxe-Coburg Publications, Stirlingshire, Scotland, 2012.

[3] K.J. Bathe, "Insights and Advances in the Analysis of Structures", in "Proceedings of the Fifth International Conference on Structural Engineering, Mechanics and Computation, University of Cape Town", A. Zingoni, (Editor), Taylor & Francis, 2013.

[4] K.J. Bathe, "Finite Element Procedures", Second edition, 2014.

[5] D. J. Payen and K.J. Bathe, "A Stress Improvement Procedure", Computers & Structures, 112-113, 311-326, 2012.

[6] J.H. Kim and K.J. Bathe, "The Finite Element Method Enriched by Interpolation Covers", Computers & Structures, 116, 35-49, 2013.

[7] J.H. Kim and K.J. Bathe, "Towards a Procedure to Automatically Improve Finite Element Solutions by Interpolation Covers", Computers & Structures, 131, 81-87, 2014.
[8] H.M. Jeon, P.S. Lee and K.J. Bathe, "The MITC3 Shell Finite Element Enriched by Interpolation Covers", Computers & Structures, 134, 128-132, 2014.
[9] Y. Lee, P.S. Lee and K.J. Bathe, "The MITC3+ shell element and its performance", Computers & Structures, 138, 12-23, 2014.
[10] H.M. Jeon, Y. Lee, P.S. Lee and K.J. Bathe, "The MITC3+ shell element in large deformations", Computers & Structures, submitted.
[11] P.S. Lee and K.J. Bathe, "Development of MITC Isotropic Triangular Shell Finite Elements", Computers & Structures, 82, 945-962, 2004.
[12] D. Chapelle and K.J. Bathe, "Fundamental Considerations for the Finite Element Analysis of Shell Structures", Computers & Structures, 66, 19-36, 711-712, 1998.
[13] D. Chapelle, and K.J. Bathe, "The Finite Element Analysis of Shells – Fundamentals", Second edition, Springer, 2011.
[14] K.J. Bathe, "Conserving energy and momentum in nonlinear dynamics: A simple implicit time integration scheme", Computers & Structures, 85, 437-445, 2007.
[15] K. J. Bathe and M. M. I. Baig, "On a Composite Implicit Time Integration Procedure for Nonlinear Dynamics", Computers & Structures, 83, 2513 – 2534, 2005.
[16] K. J. Bathe and G. Noh, "Insight into an Implicit Time Integration Scheme for Structural Dynamics", Computers & Structures, 98-99, 1-6, 2012.
[17] G. Noh, S. Ham and K. J. Bathe**, "**Performance of an Implicit Time Integration Scheme in the Analysis of Wave Propagations", Computers & Structures, 123, 93-105, 2013.
[18] G. Noh and K.J. Bathe, "An Explicit Time Integration Scheme for the Analysis of Wave Propagations", Computers & Structures, 129, 178-193, 2013.
[19] T. Sussman and K.J. Bathe, "3D-shell Elements for Structures in Large Strains", Computers & Structures, 122, 2-12, 2013.
[20] Z. Kazanci and K.J. Bathe, "Crushing and Crashing of Tubes with Implicit Time Integration", Int. J. Impact Engineering, 42, 80-88, 2012.
[21] S. Ham and K.J. Bathe, "A Finite Element Method Enriched for Wave Propagation Problems", Computers & Structures, 94-95, 1-12, 2012.
[22] S. Ham, B. Lai and K.J. Bathe, "The Method of Finite Spheres Enriched for Wave Propagation Problems", Computers & Structures, 142, 1-14, 2014.
[23] K.J. Bathe, "The Subspace Iteration Method – Revisited", Computers & Structures, 126, 177-183, 2013.
[24] K.J. Bathe and J. Dong, "Component Mode Synthesis with Subspace Iterations for Controlled Accuracy of Frequency and Mode Shape Solutions", Computers & Structures, 139, 28-32, 2014.
[25] K.J. Bathe, H. Zhang and Y. Yan, "The Solution of Maxwell's Equations in Multiphysics", Computers & Structures, 132, 99-112, 2014.

[26] K.J. Bathe and H. Zhang, "A Flow-Condition-Based Interpolation Finite Element Procedure for Incompressible Fluid Flows", Computers & Structures, 80, 1267-1277, 2002.
[27] K.J. Bathe and H. Zhang, "Finite Element Developments for General Fluid Flows with Structural Interactions", Int. Journal for Numerical Methods in Engineering, 60, 213-232, 2004.
[28] K.J. Bathe and H. Zhang, "A Mesh Adaptivity Procedure for CFD and Fluid-structure Interactions", Computers & Structures, 87, 604-617, 2009.
[29] M. Bathe, "A Finite Element Framework for Computation of Protein Normal Modes and Mechanical Response", Proteins: Structure, Function and Bioinformatics, 70, 1595-1609, 2008.
[30] R.S. Sedeh, M. Bathe, and K.J. Bathe, "The Subspace Iteration Method in Protein Normal Mode Analysis", J. Computational Chemistry, 31, 66-74, 2010.
[31] R.S. Sedeh, O. Hallatschek, M. Bathe and K.J. Bathe, "Finite Element Framework for Brownian Dynamics of High Molecular Weight Proteins and Protein Assemblies", in preparation.
[32] D.N. Kim, F. Kilchherr, H. Dietz and M. Bathe, "Quantitative Prediction of 3D Solution Shape and Flexibility of Nucleic Acid Nanostructures", Nucleic Acids Research, 40, 2862-2868, 2012.
[33] R.S. Sedeh, M. Adendorff, O. Hallatschek, K.J. Bathe and M. Bathe, "Brownian Dynamics of DNA Nanostructures", in preparation.
[34] C.E. Castro, F. Kilchherr, D.N. Kim, E. Lin Shiao, T. Wauer, P. Wortmann, M. Bathe and H. Dietz," A Primer to Scaffolded DNA Origami", Nature Methods, 8, 221-229, 2011.
[35] T. Sussman and K. J. Bathe, "Spurious Modes in Geometrically Nonlinear Small Displacement Finite Elements with Incompatible Modes", Computers & Structures, 140, 14-22, 2014.
[36] M.L.Bucalem and K.J. Bathe, "The Mechanics of Solids and Structures – Hierarchical Modeling and the Finite Element Solution", Springer, 2011.